

4-(3-((Pyridin-4-ylmethyl)amino)-[1,2,4]triazolo[4,3-b][1,2,4]triazin-6-yl)phenol: an improved anticancer agent in hepatocellular carcinoma and a selective MDR1/MRP modulator

Article

Accepted Version

Khatir, Z. Z., Di Sotto, A., Percaccio, E., Kucukkilinc, T. T., Ercan, A., Chippindale, A. M. ORCID: <https://orcid.org/0000-0002-5918-8701>, Valipour, M. and Irannejad, H. (2024) 4-(3-((Pyridin-4-ylmethyl)amino)-[1,2,4]triazolo[4,3-b][1,2,4]triazin-6-yl)phenol: an improved anticancer agent in hepatocellular carcinoma and a selective MDR1/MRP modulator. *Archiv de Pharmazie*, 2024. e2300704. ISSN 1521-4184 doi: <https://doi.org/10.1002/ardp.202300704> Available at <https://centaur.reading.ac.uk/115649/>

It is advisable to refer to the publisher's version if you intend to cite from the work. See [Guidance on citing](#).

To link to this article DOI: <http://dx.doi.org/10.1002/ardp.202300704>

Publisher: Wiley

including copyright law. Copyright and IPR is retained by the creators or other copyright holders. Terms and conditions for use of this material are defined in the [End User Agreement](#).

www.reading.ac.uk/centaur

CentAUR

Central Archive at the University of Reading

Reading's research outputs online

4-(3-((Pyridin-4-ylmethyl)amino)-[1,2,4]triazolo[4,3-*b*][1,2,4]triazin-6-yl)phenol: an improved anticancer agent in hepatocellular carcinoma and a selective MDR1/MRP modulator

Zahra Zakeri Khatir¹, Antonella Di Sotto², Ester Percaccio², Tuba Tuylu Kucukkilinc³, Ayse Ercan³, Ann M. Chippindale⁴, Mehdi Valipour⁵, Hamid Irannejad^{1}*

¹*Department of Medicinal Chemistry, Faculty of Pharmacy, Mazandaran University of Medical Sciences, Sari, Iran*

²*Department of Physiology and Pharmacology "V. Erspamer", Sapienza University of Rome, P. le Aldo Moro 5, 00185 Rome, Italy*

³*Department of Biochemistry, Faculty of Pharmacy, Hacettepe University, Sıhhiye, Ankara 06100, Turkey*

⁴*Department of Chemistry, University of Reading, Whiteknights, Reading, Berks, RG6 6DX, UK*

⁵*Razi Drug Research Center, Iran University of Medical Sciences, Tehran 14496-14535, Iran*

*Author for correspondence: irannejadhamid@gmail.com. [ORCID ID: 0000-0001-7513-6162](https://orcid.org/0000-0001-7513-6162)

Abstract: Hepatocellular carcinoma is the most common type of primary liver cancer. However, multidrug resistance (MDR) is a major obstacle to the effective chemotherapy of cancer cells. This report documents the rational design, synthesis and biological evaluation of a novel series of triazolotriazines substituted with CH₂NH-linked pyridine for use as dual c-Met/MDR inhibitors. The compound **12g** with IC₅₀ of 3.06 μM on HepG2 cells showed more potency than crizotinib (IC₅₀ = 5.15 μM) in MTT assay. In addition, **12g** inhibited c-Met kinase at low micromolar level (IC₅₀ = 0.052 μM). **12g** significantly inhibited Pgp and MRP1/2 efflux pumps in both cancerous HepG2 and BxPC3 cells starting from the lower concentrations of 3 and 0.3 μM, respectively. **12g** did not inhibit MDR1 and MRP1/2 in noncancerous H69 cholangiocytes up to the concentration of 30 and 60 μM, respectively. Current results highlighted that cancerous cells were more susceptible to the effect of **12g** than normal cells, in which the inhibition occurred only at the highest concentrations, suggesting a further interest in **12g** as a selective anticancer agent. Overall, **12g**, as a dual c-Met and P-gp/MRP inhibitor, is a promising lead compound for developing a new generation of the anticancer agents.

Keywords: triazolotriazine, c-Met kinase inhibitor, multidrug resistance, MDR1, MRP1/2

1. Introduction

Mesenchymal-epithelial transition factor (c-Met), also known as hepatocyte growth factor receptor (HGFR), is one of the receptor tyrosine kinases that manages several cellular processes via phosphorylation. Binding of HGF to the receptor leads to diverse intracellular processes, such as angiogenesis, proliferation, migration, and invasion. Over-expression and mutation of c-Met can lead to various organ cancers. Regardless of significant progress in developing selective c-Met inhibitors, resistance and mutagenesis forced researchers to develop new c-Met inhibitors with drug-like properties and efficacy [1]. Resistance to chemotherapeutic agents in the later stages of the disease is one of the most significant challenges in cancer treatment. Drug efflux pumps are one of several molecular mechanisms related to drug resistance that impede cancer treatment success [2]. This mechanism is exemplified by the mammalian multidrug resistance (MDR) system, which is mediated mostly by P-glycoprotein (P-gp) encoded by the MDR1 (also known as ABCB1 or ATP Binding Cassette Subfamily B member 1) gene. Other studies also identified multidrug resistance protein 1 (MRP1)/ATP Binding Cassette Subfamily C member 1 (ABCC1) and breast cancer resistance protein (BCRP)/ABC Subfamily G member 2 (ABCG2) as the molecular targets involved in cancer drug resistance [3].

P-glycoprotein as the product of the MDR1 gene, is the first identified and the most studied ATP-dependent transporter because of the broadest substrate specificity, tissue and organ distribution. P-gp, MRP1 and BCRP are the three most implicated transporters in cancer drug resistance [4].

Our previous study showed that P-gp has a wide substrate specificity and has several substrate binding domains which depends mainly on the lipophilicity and the size of the molecular structure. Our previous results further indicated that the bottom of the funnel shape formed by

the transmembrane helices and also nucleotide binding domains (NBD) are the putative substrate binding sites of P-gp [5], [6]. Some c-Met tyrosine kinase inhibitors, such as glesatinib, crizotinib, tivantinib, and tepotinib, which are either approved or currently in clinical trials, have an MDR reversal effect by regulating P-gp [7], [8], [9], [10].

In our previous study, some benzimidazole-substituted triazolotriazines (Compound **1**, Figure 1) were synthesized and showed anticancer effect in hepatocellular carcinoma. They showed trivial inhibition of the c-Met but maintained moderate hepatocellular adenocarcinoma toxicity [11]. In order to optimize their binding affinity towards the c-Met, thiomethylpyridine hinge binders (Compound **2**, Figure 1) were previously designed in our group and showed potent c-Met tyrosine kinase inhibition potential [12].

Due to their low solubility in the aqueous biologic medium and to eliminate the sulfur oxidation at a labile metabolic site, NH-replacement analogs were considered for synthesis and further evaluation to improve solubility and metabolic stability and also to confer MDR activity. Herein, a series of target compounds **11a-g** and **12a-g** with 6-aryl-[1,2,4]triazolo[4,3-b][1,2,4]triazines linked through aminomethylene to 3- or 4-pyridyl rings were designed and synthesized as possible dual c-Met and MDR modulators (Figure 1).

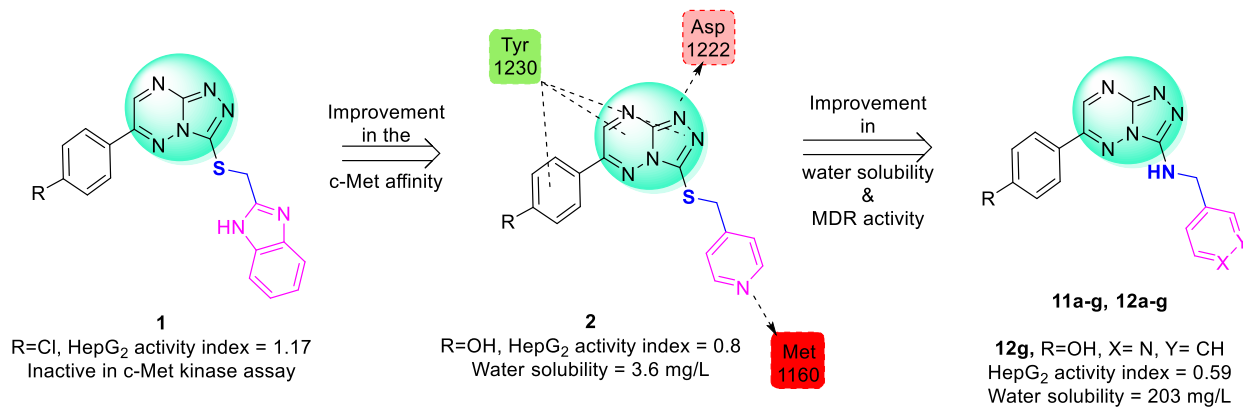


Figure 1. Design strategy and general structure of the target compounds based on our previously synthesized compounds. HepG2 activity index is defined as the IC₅₀ of the compound divided by the IC₅₀ of crizotinib in the same experiment of HepG2 MTT assay. By applying the new structural modification, water solubility of the new compound **12g** was increased by more than 56 fold.

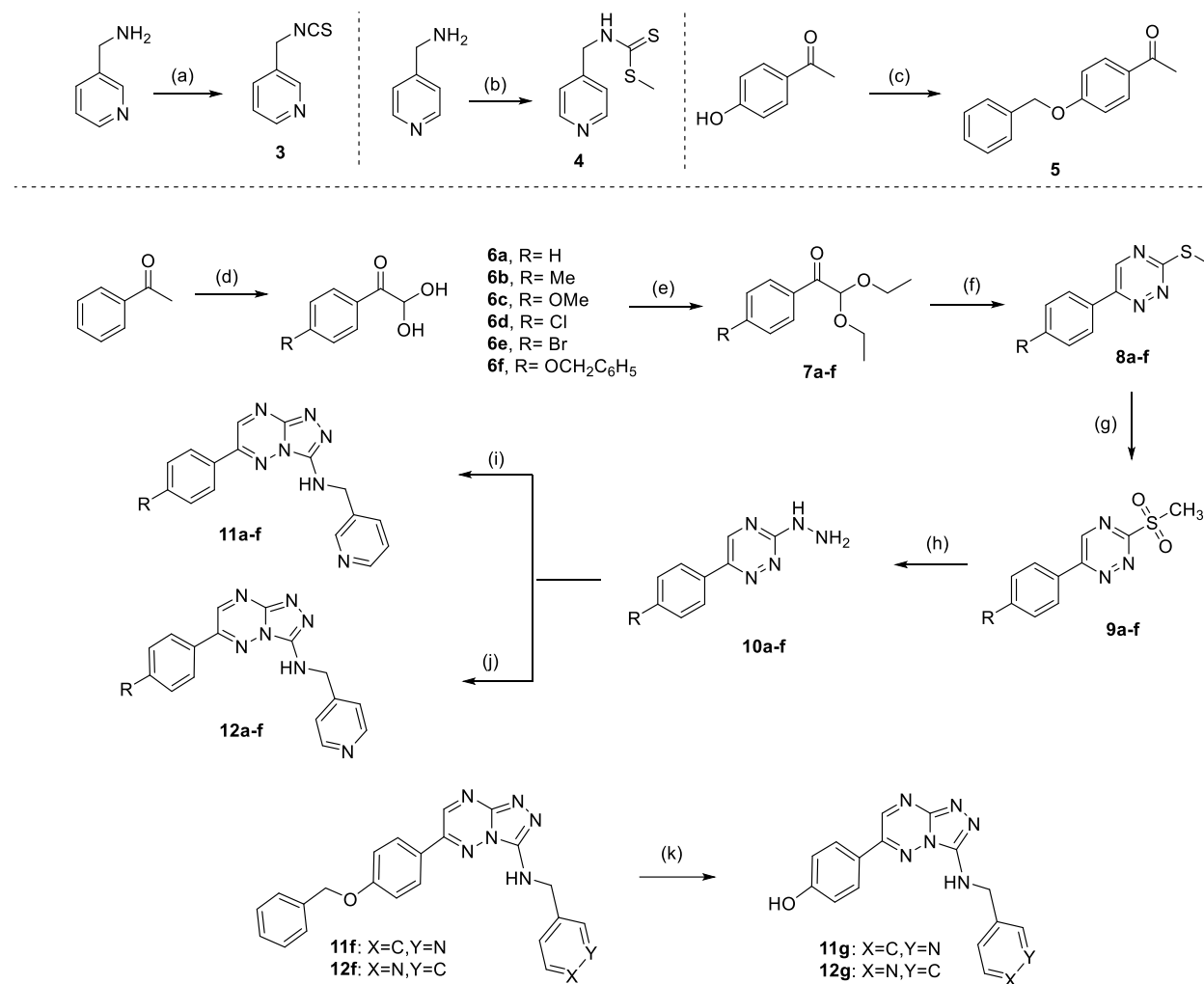
2. Results & discussion

2.1. Chemistry

The synthetic steps used to prepare the novel triazolotriazines are summarized in Scheme 1. Initially, the oxidation of acetophenone derivatives by HBr in DMSO afforded compounds (**6a-f**) [13]. Then intermediates (**7a-f**) were prepared by refluxing compounds (**6a-f**) with triethyl orthoformate in the presence of *p*-toluenesulfonic acid (PTSA) in dichloromethane. Treating intermediates (**7a-f**) with thiosemicarbazide and PTSA in ethanol, followed by methylation of the thiosemicarbazide thiol groups with iodomethane was performed sequentially *in situ*. The 1,2,4-triazine formation was accomplished in the subsequent reaction by stirring at 60 °C with acetic acid overnight to afford **8a-f**. In the next step, sulfur oxidation of compounds (**8a-f**) was performed by oxone in H₂O/THF to give compounds (**9a-f**). Stirring of compounds (**9a-f**) in THF in the presence of hydrazine hydrate gave (**10a-f**) in acceptable yield [12]. Finally, reaction of the intermediates (**10a-f**) with either 3-(isothiocyanatomethyl) pyridine (**3**) or methyl (pyridine-4-ylmethyl) carbamidothioate (**4**) in the presence of dicyclohexylcarbodiimide (DCC) in ethanol led to the final compounds (**11a-f**) and (**12a-f**), respectively [14]. The 4-hydroxy analogs, **11g** and **12g**, were then prepared by debenzoylation of their corresponding analogs, **11f** and **12f**, in acidic conditions [15]. Column chromatography was used to purify the final compounds, and their chemical structures were confirmed using spectral data (¹H NMR, ¹³C NMR and mass spectrometry) and single-crystal X-ray crystallography.

The water solubility of compounds **2**, **11b** and **12g** were determined in deionized water. Results revealed that compounds **11b** and **12g** with water solubility of 25.26 mg/L and 203.53 mg/L

have much higher solubility in water compared to compound **2** (3.60 mg/L). Therefore, our suggested design concept of improving water solubility by introducing a suitable polar group to the novel compounds was entirely confirmed.



Scheme 1. Synthetic pathways for triazolotriazine derivatives **11a-g** and **12a-g**. Reagents and conditions: **(a)** step 1) CS₂, H₂O, K₂CO₃, stir, overnight, rt, step 2) Cyanuric chloride, stir; **(b)** step 1) CS₂, Et₃N, stir, rt, step 2) MeI, stir; **(c)** Benzyl chloride, DMF, stir, overnight, rt; **(d)** step 1) DMSO, HBr, stir, 60 °C, step 2) H₂O, reflux; **(e)** Triethyl orthoformate, p-TsOH.H₂O, CH₂Cl₂, reflux; **(f)** step 1) Thiosemicarbazide, EtOH, p-TsOH.H₂O, stir, 4h, step 2) CH₃I, rt, stir, step 3) CH₃COOH, 60 °C; **(g)** Oxone, H₂O, THF, stir, rt; **(h)** NH₂NH₂.H₂O, THF, stir, rt; **(i)** step 1) Compound **3**, EtOH, reflux, 1h, step 2) DCC, reflux, overnight; **(j)** step 1) Compound **4**, EtOH, reflux, overnight, step 2) DCC, reflux, overnight; **(k)** HCl, CH₃COOH, 3h reflux.

2.1.1. X-ray crystallography of **11c**

An ORTEP diagram of the structure of compound **11c**, as determined by single-crystal X-ray diffraction, indicating the labeling of the one molecule in the asymmetric unit is presented in Figures 2 and S1. Crystallographic data and experimental details for compound **11c** are reported in Table S1. The results showed that the molecules stack parallel to the *c* axis and are held together by face-to-face π - π stacking interactions (Figure S2). The ring-centroid separation $C_g(C(2) - C(3) - C(4) - C(5) - C(23) - C(24)) \cdots C_g(C(6) - N(7) - N(8) - C(9) - N(10) - C(11))$ is 3.429(2) Å and the shortest distance between the centroid of one ring and the plane of the other is 3.339(2) Å. In addition, hydrogen bonding interactions (N(15) - H(151) \cdots N(12), 3.0874(16) Å) connect neighbouring molecules together along the *a* axis (Figure S5). Crystallographic details are given in Cambridge Crystallographic Data Centre, deposit code CCDC 2192826.

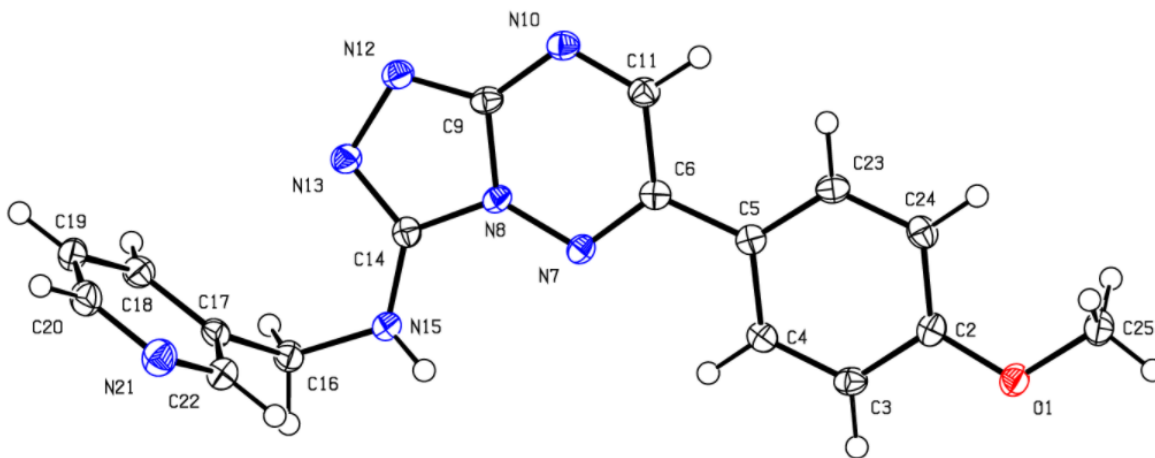


Figure 2. ORTEP diagram of the molecular structure of compound **11c**, as determined by single-crystal X-ray diffraction: asymmetric unit with labeling scheme. Thermal ellipsoids are shown at 50% probability.

2.1.2. Spectral data

Target compounds **11a-g** and **12 a-g** were characterized using ^1H and ^{13}C NMR and the details are summarized in Table S6. The triplets at 5.84-7.80 and 5.47-7.91 ppm in the ^1H NMR spectra of compounds **11a-g** and **12a-g**, respectively are related to the NH group, whereas in **11d** and **11e**, the same proton appears as a multiplet. Generally, the ^1H NMR spectra of compounds (**11a-g**) and (**12 a-g**) show a doublet signal in the region of 4.64-4.96 and 4.65-4.89 ppm, respectively, which are related to the aliphatic- CH_2 group. Specially, the C7-H proton of the triazine ring appeared as a singlet in the region of 8.78-9.07 and 8.79-9.09 ppm in the **11a-g** and **12 a-g** series of compounds respectively. The ^{13}C NMR spectra showed one signal at 43.59-43.99 and 44.69-44.90 ppm for **11a-g** and **12a-g** corresponding to the aliphatic- CH_2 group. The other ^{13}C signals could be attributed to the carbons of aromatic rings. In their mass spectra, the expected molecular ion peak was observed at high intensity for all compounds. In addition, bromo- and chloro-isotope fragments were seen in **11d**, **11e**, **12d** and **12e**, further confirming the compounds' structures. The m/z of 173.1 was also observed in the most of the mass spectra corresponding to the fragment $\text{C}_8\text{H}_7\text{N}_5^{2+}$ (Figure 3).

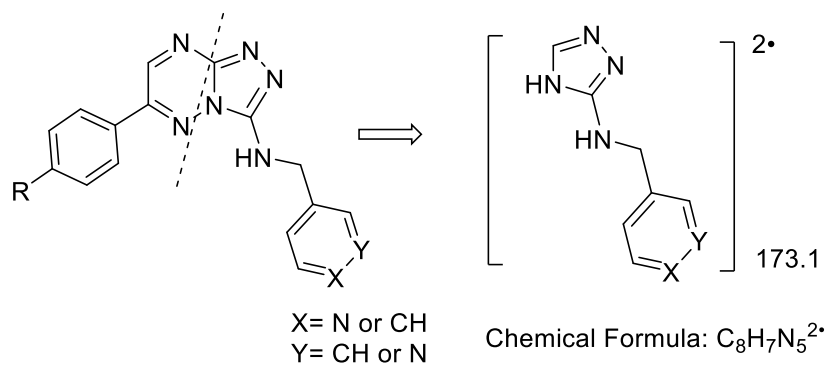


Figure 3. The important ion-fragment, $\text{C}_8\text{H}_7\text{N}_5^{2+}$, identified in the final compounds **11a-g** and **12a-g**.

2.2. Biological evaluation

2.2.1 HGF-induced proliferation assay

All the target compounds, **11a-g** and **12a-g**, were tested for their antitumor activity against HGF-induced c-Met expressing human cancer cell lines, MCF7 (Human hormone receptor-positive breast cancer cell line), HepG2 (human liver cancer cell line), HT-29 (human colon cancer cell line) and MDA-MB-231 (Human triple-negative breast cancer cell line) by MTT assay and the results were compared with crizotinib. In addition, mouse fibroblast non-cancerous cell line L929 was treated with the target compounds in order to assess their selectivity on normal tissue (Table 1). The results indicate that all the synthesized compounds, **11a-g** and **12a-g**, had moderate-to-strong cytotoxicity with IC_{50} values ranging from 3.059 to 33.61 μ M upon the treatment in the four cell lines. It was also found that the target compounds were non-toxic against the non-cancerous cell line L929 at 25 and 50 μ M concentrations (percent of viability in the range of 63.2-108.5%).

Compounds **12f** and **12g** were found to be the most potent compounds in the series and showed high potency for inhibiting HepG2 cells. The antitumor activity of **12f** (HepG2 IC_{50} = 5.736 μ M) was comparable to that of the reference drug, crizotinib (IC_{50} = 5.15 μ M). Interestingly, **12g** demonstrated remarkable inhibitory activity against the HepG2 cell line with IC_{50} value equal 3.06 μ M and was more potent than, crizotinib.

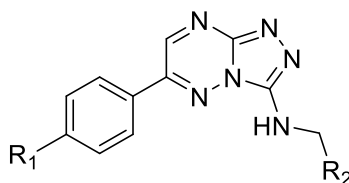
In the case of MDA-MB-231 cancer cells, analogs **11a** and **11f** showed higher activity than their congeners with IC_{50} values of 11.35 and 12.21 μ M, respectively. Moreover, the target compounds showed moderate cytotoxicity on MCF7 cancer cell lines, and their IC_{50} values were in the range of 15.5-26.2 μ M. None of the target molecules were more cytotoxic than crizotinib (IC_{50} = 6.65 μ M) on MCF7 cells. In addition, compound **12d** was the most potent compound on the HT-29 cell line, with an IC_{50} value of 9.6 μ M.

There is not a significant difference in potency between the target compounds regarding the type of the R₁ substituent on the *para* position of the phenyl ring. The anticancer activity of the compounds does not appear to relate to the size or the electron-donating/withdrawing property of the substituents. In spite of observing that the most potent compounds, **12f** and **12g**, are among the 4-pyridyl substituted analogs, there is not a significant difference or any trend observed for the antitumor activity of the 3- or 4-pyridyl- substituted target compounds.

According to our previously published results, the pyridine-linked triazolotriazine congeners and benzimidazolyl/benzoxazolyl-linked triazolotriazines have excellent anticancer activity against HepG2 cells in low micro-molar concentrations [11], [12]. Notably, the current results obtained by the new congeners further confirm our previous observations. To better compare the anticancer activity of our current and previously synthesized compounds against HepG2 cells, an index of HepG2 activity was introduced and defined as the IC₅₀ of the tested compound divided by the IC₅₀ of crizotinib, obtained in the same MTT assay. The lower value of this index, the more potent the compound.

As shown in Figure 1, the HepG2 activity index decreased from 1.17 (compound **1**) to 0.8 (compound **2**) and further to 0.59 for the currently synthesized compound **12g** which confirms the improvement in the HepG2 cellular anticancer activity of the series.

Table 1. Cytotoxicity of the target compounds against HGF-induced MTT assay on HT-29, HepG2, MCF7 and MDA-MB-231 cancer cells. Mouse fibroblast non-cancerous cell line L929 were used without HGF induction for assessing basal cytotoxicity.



Compd	R ₁	R ₂	IC ₅₀ (μM)				L929 (%viability) ^a
			HT29	HepG2	MCF7	MDA-MB 231	
11a	H	3-Pyridyl	19.8±1.06	16.66±1.15	24.82±1.11	11.35±1.11	93.0±7.0
11b	Me	3-Pyridyl	16.31±1.07	17.2±1.17	26.21±1.07	20.22±1.07	96.4±7.0
11c	OMe	3-Pyridyl	16.42±1.07	14.88±1.15	21.20±1.08	13.88±1.11	93.1±8.5
11d	Cl	3-Pyridyl	18.98±1.03	16.75±1.20	22.75±1.13	17.12±1.06	86.7±10.3
11e	Br	3-Pyridyl	20.11±1.06	16.35±1.14	15.55±1.09	13.74±1.09	63.2±6.6
11f	OCH ₂ C ₆ H ₅	3-Pyridyl	30.48±1.06	13.84±1.24	21.93±1.07	12.21±1.12	98.0±7.3
11g	OH	3-Pyridyl	13.26±1.14	16.64±1.14	17.99±1.15	16.93±1.06	108.5±3.3
12a	H	4-Pyridyl	14.91±1.07	26.39±1.10	25.23±1.18	22.49±1.07	94.9±5.1
12b	Me	4-Pyridyl	15.6±1.08	20.86±1.13	24.08±1.15	17.49±1.12	89.9±7.9
12c	OMe	4-Pyridyl	16.25±1.11	33.61±1.13	18.79±1.12	15.55±1.2	95.2±4.6
12d	Cl	4-Pyridyl	9.62±1.14	19.61±1.12	23.63±1.07	23.16±1.08	90.2±3.2
12e	Br	4-Pyridyl	10.06±1.18	19.95±1.13	21.44±1.12	17.23±1.09	95.5±3.5
12f	OCH ₂ C ₆ H ₅	4-Pyridyl	11.62±1.11	5.73±1.19	17.37±1.09	17.02±1.11	91.2±12.5
12g	OH	4-Pyridyl	12.4±1.13	3.06±1.18	19.30±1.09	16.85±1.07	87.9±11.4
Crizotinib			8.08±1.10	5.15±1.22	6.65±1.17	6.49±1.08	89.9±3.2

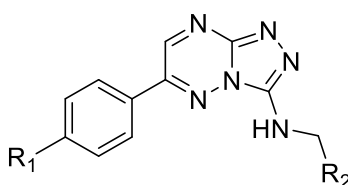
^a Percent viability of normal L929 cells in 25 μM concentration of compounds. Data presented is the mean ± SD value from three separate experiments. The values in bold are discussed in the text.

2.2.2 c-Met kinase assay

The flexible aminomethylene side chain containing a pyridine moiety serves as a hinge binder to ensure the formation of an essential hydrogen bond with Met1160 in the putative binding site of the c-Met kinase. Accordingly, all the target compounds, **11a-g** and **12a-g**, were screened for c-Met kinase inhibition activity using the c-Met Kinase Enzyme System assay employing crizotinib as a reference drug. As summarized in Table 2, all the compounds tested demonstrated

notable c-Met kinase inhibition with IC₅₀ values ranging from 0.052-26.9 μM. Surprisingly, **12g** again emerged as the most potent c-Met inhibitor with an IC₅₀ value of 0.052 μM in the series, while the IC₅₀ of crizotinib was 0.012 μM. Interestingly, **11e** was found to be the second most potent compound for c-Met inhibition showing IC₅₀ of 0.062 μM, and the most potent compound towards MCF7 tumor cells. Overall, **12g**, with the 4-pyridyl group, showed superior activity among the compounds investigated.

Table 2. c-Met kinase inhibition potential of **11a-g** and **12a-g**.



Compd	R ₁	R ₂	c-Met kinase IC ₅₀ (μM)
11a	H	3-Pyridyl	0.958±0.55
11b	Me	3-Pyridyl	1.05±0.44
11c	OMe	3-Pyridyl	3.70±1.19
11d	Cl	3-Pyridyl	5.65±0.83
11e	Br	3-Pyridyl	0.062±0.01
11f	OCH ₂ C ₆ H ₅	3-Pyridyl	0.935±0.40
11g	OH	3-Pyridyl	1.23±0.48
12a	H	4-Pyridyl	14.96±2.14
12b	Me	4-Pyridyl	26.94±6.39
12c	OMe	4-Pyridyl	0.792±0.49
12d	Cl	4-Pyridyl	13.18±4.54
12e	Br	4-Pyridyl	8.14±3.08
12f	OCH ₂ C ₆ H ₅	4-Pyridyl	2.21±1.86
12g	OH	4-Pyridyl	0.052±0.01
Crizotinib	-	-	0.0129±0.003

The values in bold are discussed in the text.

2.2.3 Modulation of MDR1 (P-glycoprotein) and MRP efflux by **12g**

Finally, **12g** was selected as the lead compound to investigate its ability to modulate the efflux mediated by MDR1 (P-glycoprotein) and MRP (multidrug resistance-associated protein) pumps

in vitro. To this end, different cell models of the hepato-biliary-pancreatic tract, including human hepatoma HepG2 cells, pancreatic adenocarcinoma Bx-PC3 cells, and noncancerous H69 intrahepatic cholangiocytes, were used for MTT assay in the absence of HGF. These cells are known to express different ABC-transporters, especially MRP1 and MRP2, along with MDR1 in the Bx-PC3 and HepG2 cells [6], [16], while MRP1 and MDR1 in noncancerous cholangiocytes [17]. The ability of the tested compound to affect the pump function was evaluated at nontoxic concentrations through the efflux assay. The intracellular accumulation of specific fluorescent substrates, including rhodamine 123 for MDR1 and calcein acetoxymethyl ester for MRPs, as a consequence of the pump inhibition by target compound was measured. Under our experimental conditions, **12g** was nontoxic up to 150 μM in all the tested cell lines; At higher concentrations, **12g** lowered the cell viability by at least 30 %, achieving the highest inhibition (60%) in HepG2 cells at the concentration of 300 μM (Figures 4A, 4C and 4E). As previously reported [18], the standard pump inhibitors verapamil and MK571 (2 μM) were also nontoxic (Figures 4B, 4D, 4F). Noteworthy, the two sections: HGF-induced proliferation assay (section 2.2.1) and MDR efflux assay were performed by the two different research teams and experts in the field and their methods of MTT assay differ. One of the basic differences is that the count of cells per well was 4000 in the HGF-induced proliferation assay, while it was 20,000 cells per well in the MDR efflux assay and in the absence of HGF (See the Methods section for the details). Another important difference between the methods is that the compound treatment duration was 72 h for the HGF-induced proliferation assay, while it was 30 min for the MDR efflux assay. As a result, **12g**, which was cytotoxic at 3 μM in the HGF-induced proliferation assay in HepG2 cells, did not reduce cell viability more than 30% in HepG2 cells at this concentration in the MDR efflux assay.

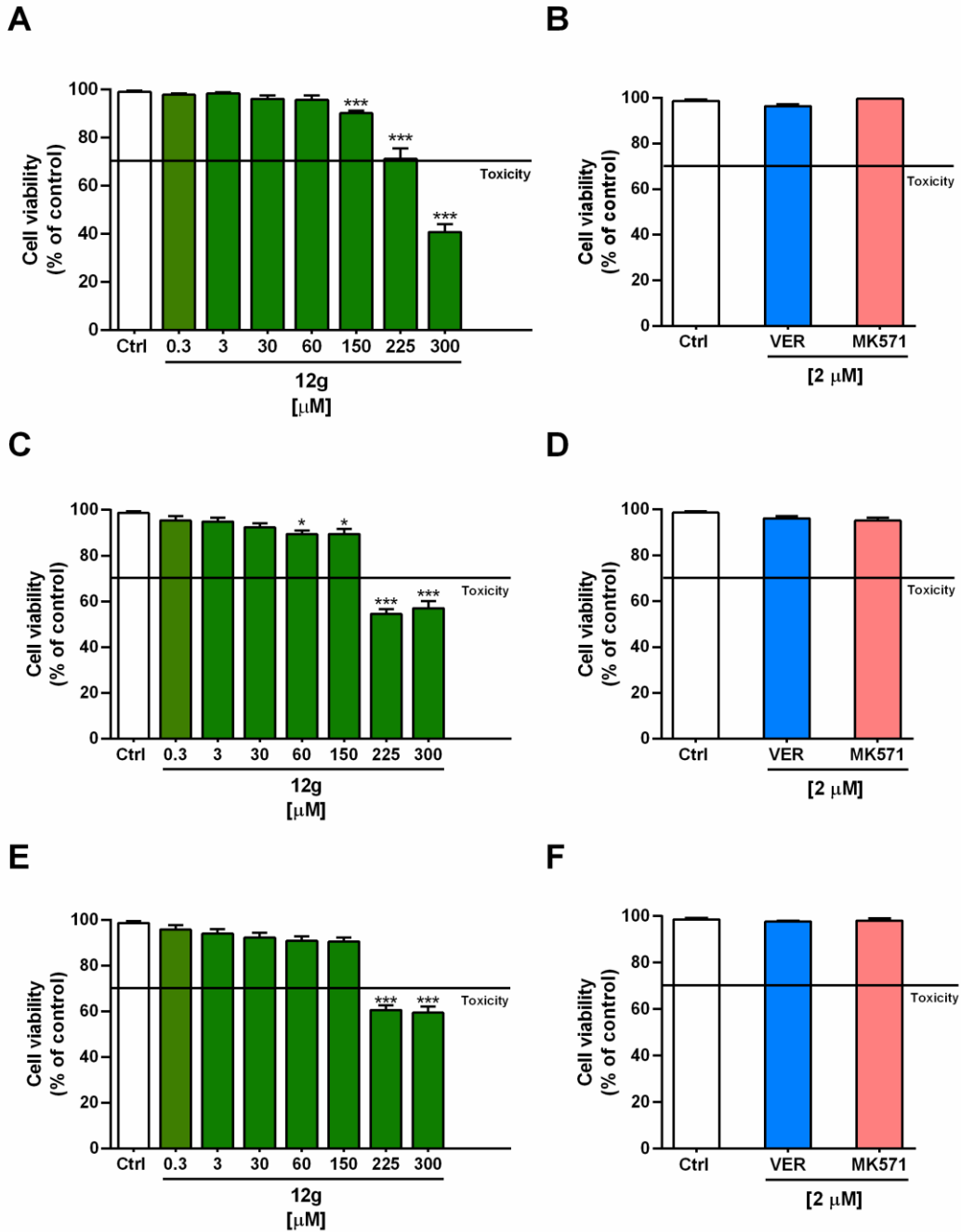


Figure 4. Cytotoxic effects of 12g, verapamil, MK571 in human hepatoma HepG2 cells (A, B), pancreatic adenocarcinoma Bx-PC3 cells (C, D) and in noncancerous H69 cholangiocytes (E, F) after 30 minutes' exposure. Data displayed as mean \pm SE of at least three independent experiments (n = 6).

Based on this preliminary evidence, the effect of **12g** on the efflux mediated by MDR1 and MRP pumps was assessed in the concentration range of 0.3-150 μM (1:2 to 1:10 dilution factor), using two specific fluorescent probes; namely, rhodamine 123 for Pgp and calcein acetoxymethyl ester for MRP1/2, respectively. According to previous studies, an increased fluorescence due to the intracellular accumulation of the probes has been evaluated as a consequence of the pump inhibition [6], [16].

Under our experimental conditions, **12g** significantly blocked Pgp and MRP1/2 pumps in both HepG2 and BxPC3 cells starting from the lower concentrations of 3 and 0.3 μM , respectively, at which points the accumulation of rhodamine 123 and calcein were both increased by about 1.2 fold (Figures 5A-5D). The block of both transporters by **12g** was progressively raised, achieving the highest effect at the concentrations of 30 μM in HepG2 cells and of 60 μM in BxPC3 cells, where the rhodamine 123 and calcein accumulations were enhanced by 1.3 and 1.2 fold, and by 1.4 and 2.7 fold, respectively (Figures 5A-5D). As expected, the positive control verapamil induced about a 1.3-fold increase of rhodamine 123 accumulation in both HepG2 and BxPC3 cells, while MK571 slightly affected the calcein accumulation in HepG2 cells, while inducing a doubling of the control levels in BxPC3 cells (Figures 5A-5D).

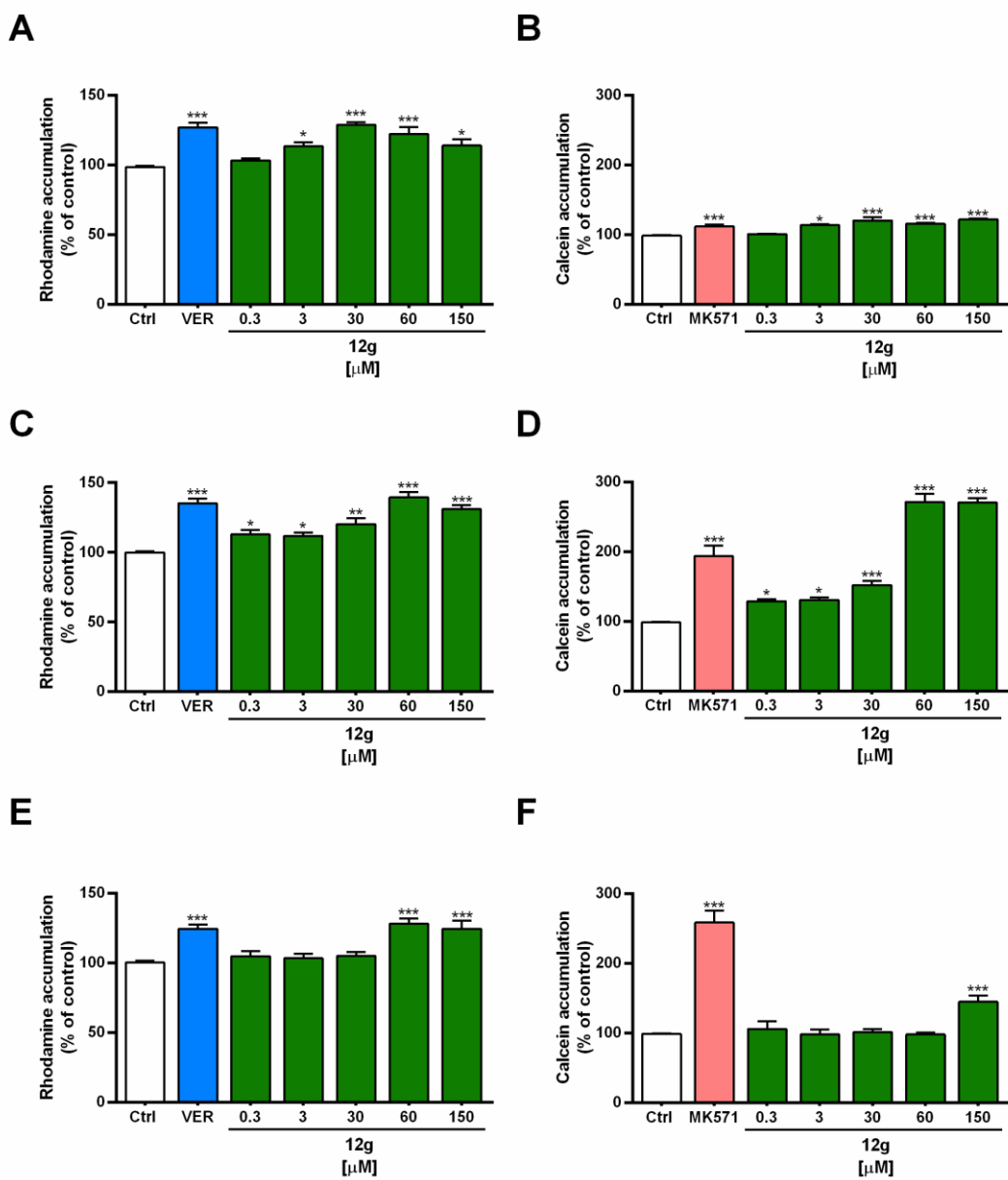


Figure 5. Effect of 12g and the standard inhibitors verapamil and MK571 on the intracellular accumulation of rhodamine 123 and calcein acetoxyethyl ester (Calcein-AM) in human hepatoma HepG2 cells (A, B), pancreatic adenocarcinoma Bx-PC3 cells (C, D) and in noncancerous H69 cholangiocytes (E, F). *** $p < 0.001$ (one-way ANOVA followed by Dunnett's Multiple Comparison Post Test) vs control.

When **12g** was assessed in noncancerous H69 cholangiocytes, it did not affect the efflux of both fluorescent probes up to the concentration of 30 μM (Figures 5E and 5F). Thus, **12g** blocked by about 1.2 fold the rhodamine 123 efflux through the MDR1 pump starting from the concentration of 60 μM . In contrast, the calcein efflux was affected by **12g** only at a concentration of 150 μM , achieving an inhibition of almost 1.5 fold (Figures 5E and 5F). According to the effects observed in H69 cholangiocytes, the positive controls, verapamil and MK571, increased the accumulations of rhodamine 123 and calcein by about 1.2- and 2.6 fold at 2 μM , respectively (Figures 5E and 5F). Overall, the current results showed that **12g** could affect the function of both MDR1 and MRP1/2 pumps, with higher potency in the cancerous HepG2 and BxPC3 cells than in the noncancerous H69 cholangiocytes, in which the inhibition occurred only at the highest concentrations tested. Therefore, the cancerous cells seem to be more susceptible to the effect of **12g** compared to the noncancerous cells. The overall results indicated that, although **12g** has lower potency than verapamil and MK571 in the inhibition of the transporters in HepG2 and BxPC3, it does not affect normal H69 cells at the same concentrations. These results show the favored selectivity of **12g**.

In order to verify the presence of the Pgp, MRP1, and MRP2 transporters in the tested cells and their modulation by **12g**, the immunofluorescence analysis using specific antibodies was also performed. The obtained results confirmed the presence of Pgp, MRP1, and MRP2 transporters in HepG2, BxPC3 and H69 cells; however, their expression was differently modulated by the treatments. (Figures 6-8). In particular, **12g** significantly increased the expression of Pgp in HepG2 and BxPC3 cells (Figures 6 and 7), and of MRP1 and MRP2 in BxPC3 cells (Figure 7). A similar trend was also shown by the positive control verapamil in HepG2 and BxPC3 cells (Figures 6 and 7), and MK571 in BxPC3 cells (Figure 7). MK571 also

increased the expression levels of MRP1 and MRP2 in H69 cholangiocytes, despite a null effect of **12g** and verapamil (Figure 8).

The increased expression of Pgp, MRP1 and MRP2 induced by **12g** in the BxPC3 cells agrees with the results of the efflux assay (Figure 5), which was affected by **12g** even at the lowest concentrations of 0.3 and 3 μ M. Similarly, at the concentration of 3 μ M, **12g** inhibited the Pgp-mediated efflux and increased the Pgp expression in HepG2 cells. Conversely, the expression of MRP1 and MRP2 was not affected, although a slight but significant inhibition of their efflux was highlighted (Figure 5). Interestingly, **12g** did not affect either the efflux function or the expression of the assayed transporters in non-cancerous H69 cells.

ABC transporters are known to mediate chemoresistance to anticancer drugs in cancer cells, leading to chemotherapy failure and tumor relapse [19]. Particularly, an upregulation of MDR1 and MRP1 in liver, biliary and pancreatic cancers has been associated with aggressive phenotype of these cancers, while the MRP2 pump seems to limit the response to anticancer drugs. A pivotal role of both MRP1 and MRP2 in the control of drug efflux from the pancreatic cells has been reported, thus increasing the interest in their modulation as a suitable strategy to counteract multidrug resistance in pancreatic cancer cells [18].

On the other hand, ABC transporters are involved in both physiological and protective functions, since they modulate the intracellular levels of xenobiotics, drugs, endogenous metabolites and toxicants, thus protecting the cells from the harmful effects of toxins. For instance, Pgp (or MDR1) can transport a wide range of structurally diverse substrates, including many drugs [17]. In contrast, MRP1 specifically mediates the efflux of neutral and anionic hydrophobic compounds and phase II metabolites, while MRP2 regulates the excretion of bilirubin and toxins [20]. Therefore, inhibiting their function in normal tissues represents a major

limitation of ABC transporter inhibitors, as it may result in the accumulation of both endogenous and exogenous toxicants, leading to serious side effects. For instance, the downregulation of the MRP2 expression has been associated to liver disfunctions and inflammation [21].

In line with this evidence, our results highlight that **12g** is able to affect the Pgp, MRP1 and MRP2 function and expression at lower concentrations in cancer cells than the normal cells, especially in pancreatic BxPC3 ones, while maintaining normal levels in H69 cholangiocytes, thereby ensuring the cell protection from xenobiotics and toxicant. This selectivity strengthens our interest in **12g** as a potential anticancer agent and encourages future in vitro and in vivo mechanistic studies.

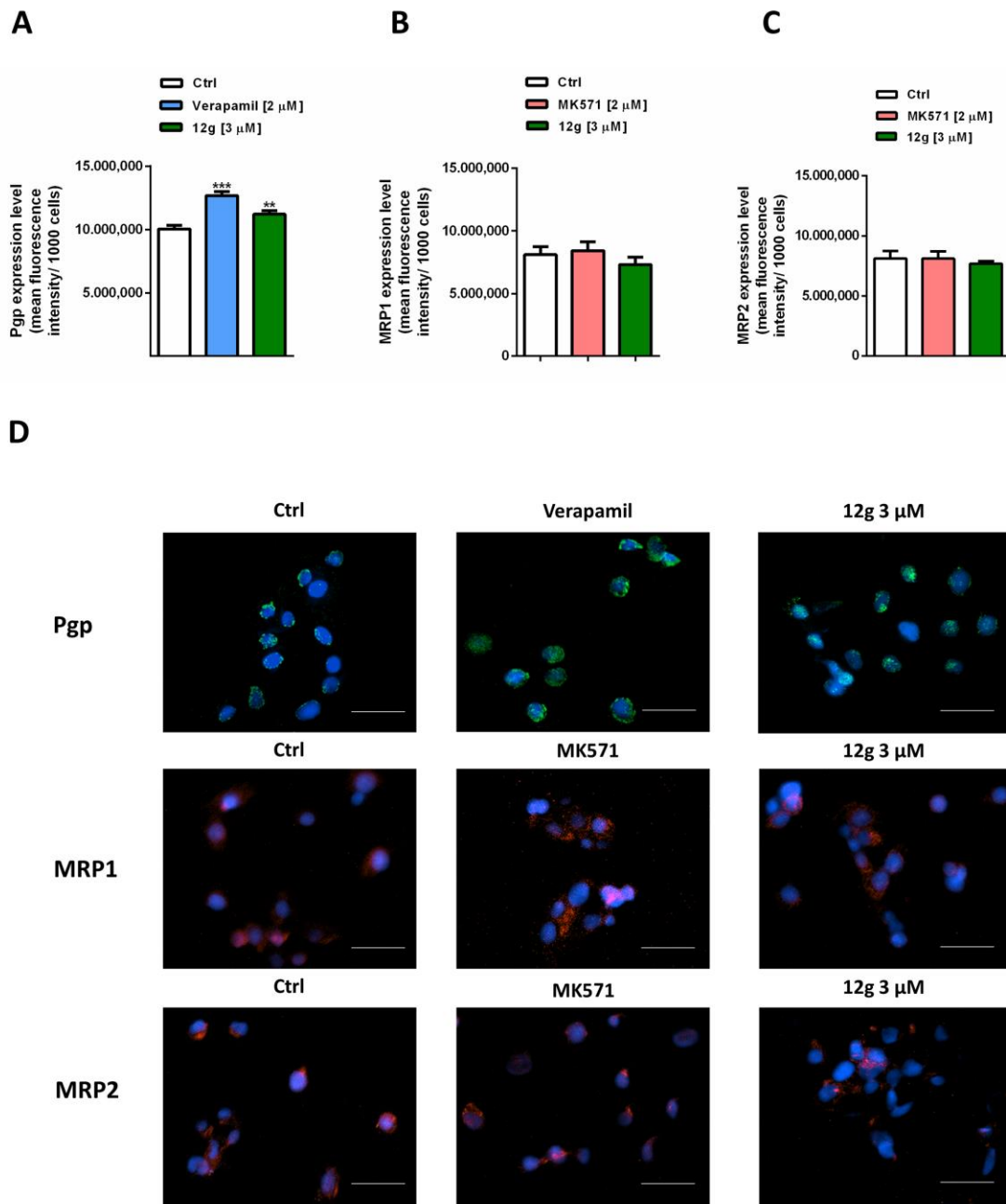


Figure 6. Modulation of the Pgp, MRP1 and MRP2 transporter expression in human hepatoma HepG2 cells by **12g** (3 μ M) and the standard inhibitors verapamil (2 μ M) and MK571 (2 μ M) after 24 h exposure. A-C) Bar graphs. Data displayed as mean \pm SE of at least two independent experiments with at least three technical replicates (n = 6). ** p < 0.01 and *** p < 0.001 (one-way ANOVA followed by Dunnett's Multiple Comparison Post Test) vs control. D) Representative images obtained at immunofluorescence analysis. Original magnification: 10X. Scale bars = 40 μ m.

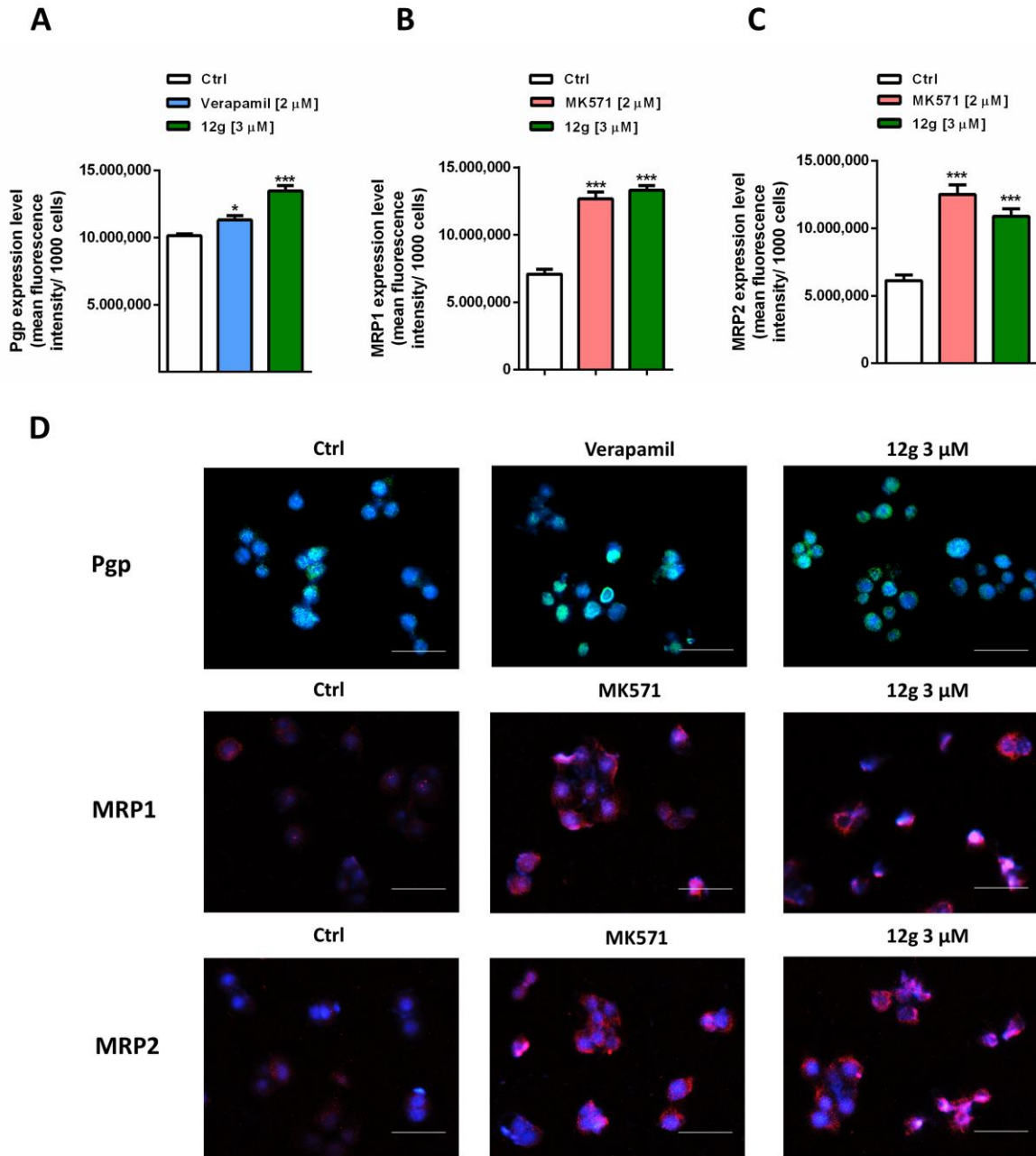


Figure 7. Modulation of the Pgp, MRP1 and MRP2 transporter expression in pancreatic adenocarcinoma Bx-PC3 cells by **12g** (3 μM) and the standard inhibitors verapamil (2 μM) and MK571 (2 μM) after 24 h exposure. A-C) Bar graphs. Data displayed as mean ± SE of at least two independent experiments with at least three technical replicates (n = 6). * p < 0.05 and *** p < 0.001 (one-way ANOVA followed by Dunnett's Multiple Comparison Post Test) vs control. D) Representative images obtained at immunofluorescence analysis. Original magnification: 10X. Scale bars = 40 μm.

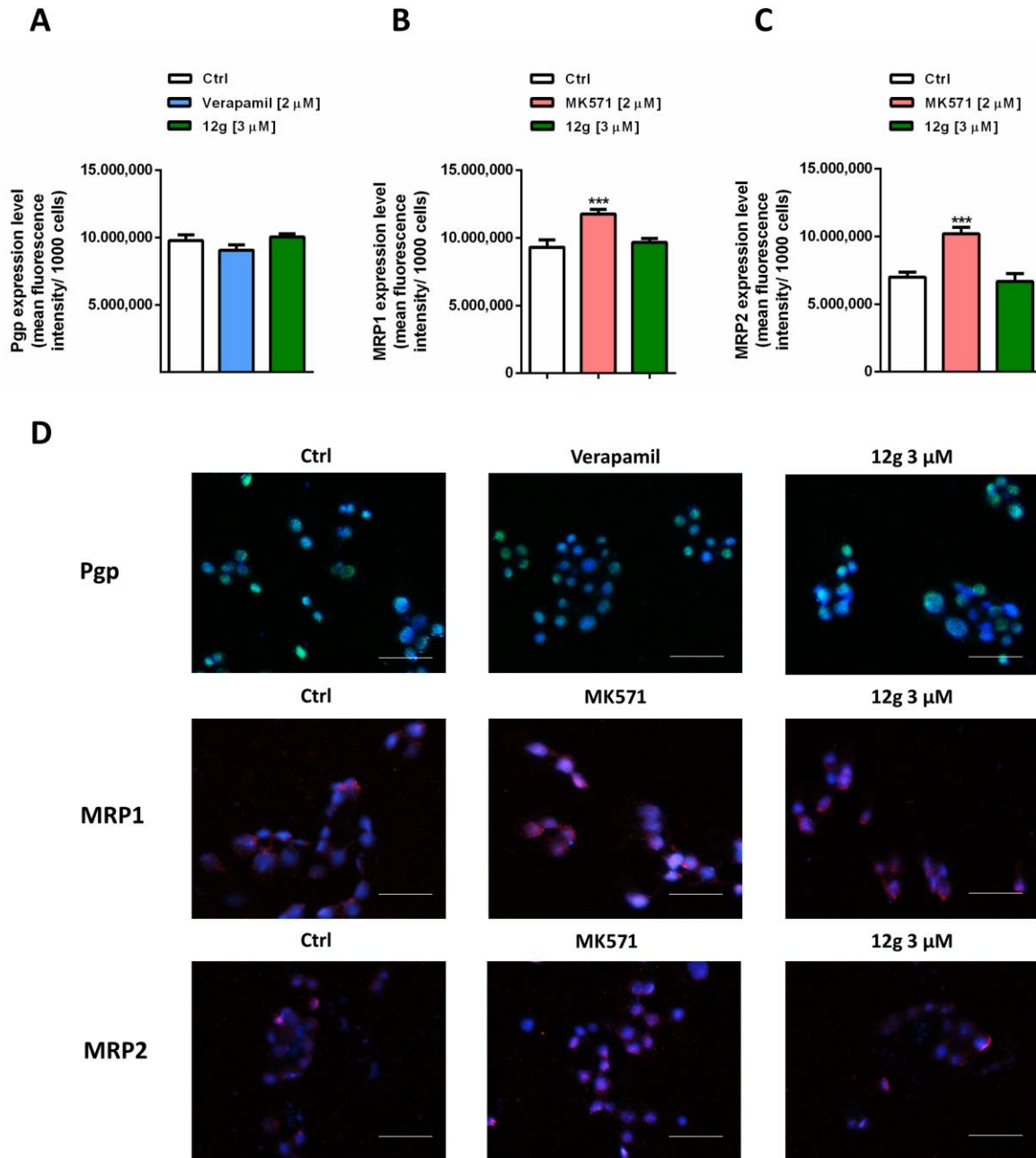


Figure 8. Modulation of the Pgp, MRP1 and MRP2 transporter expression in noncancerous H69 cholangiocytes by **12g** (3 μ M) and the standard inhibitors verapamil (2 μ M) and MK571 (2 μ M) after 24 h exposure. A-C) Bar graphs. Data displayed as mean \pm SE of at least two independent experiments with at least three technical replicates (n = 6). *** p < 0.001 (one-way ANOVA followed by Dunnett's Multiple Comparison Post Test) vs control. D) Representative images obtained at immunofluorescence analysis. Original magnification: 10X. Scale bars = 40 μ m.

2.3. *In silico studies*

To investigate the pivotal interactions for the optimal inhibition of the c-Met kinase, molecular docking and dynamics simulation experiments were performed for **12g** as this is the most promising target compound.

Compound **12g** was docked into the ATP binding site of the c-Met as a competitive inhibitor. Then, the output of docked **12g** was further studied in a 20 ns molecular dynamics simulation. The RMSD of the protein and the ligand indicate the early stabilization of the complex (Figure S5). For the analysis of the essential interactions, the last 11 frames of the simulation time were then extracted and visualized, as shown in Figures S6- S15 and in Figure 7.

The essential hydrogen bond between NH of Met1160 in the hinge region of the active site and the nitrogen atom of the pyridine ring was seen in frame numbers 2, 5, 6, 8, 10 and 11. A pi-pi stacking interaction between the triazolotriazine core of **12g** and the phenol moiety of Tyr1230 was observed in all 11 frames. A conventional hydrogen bond also exists between N4 of triazine and NH of the Asp1222 in the all extracted frames. The three mentioned bonds are key interactions reported in the literature for the optimal inhibition of the c-Met enzyme. In addition, the *p*-OH group of the phenol moiety, which is exposed to the solvent accessible area, has a hydrogen bonding interaction with the carboxylate of the Asp1231 at the entrance of the active site in frame numbers 5, 6 and 11.

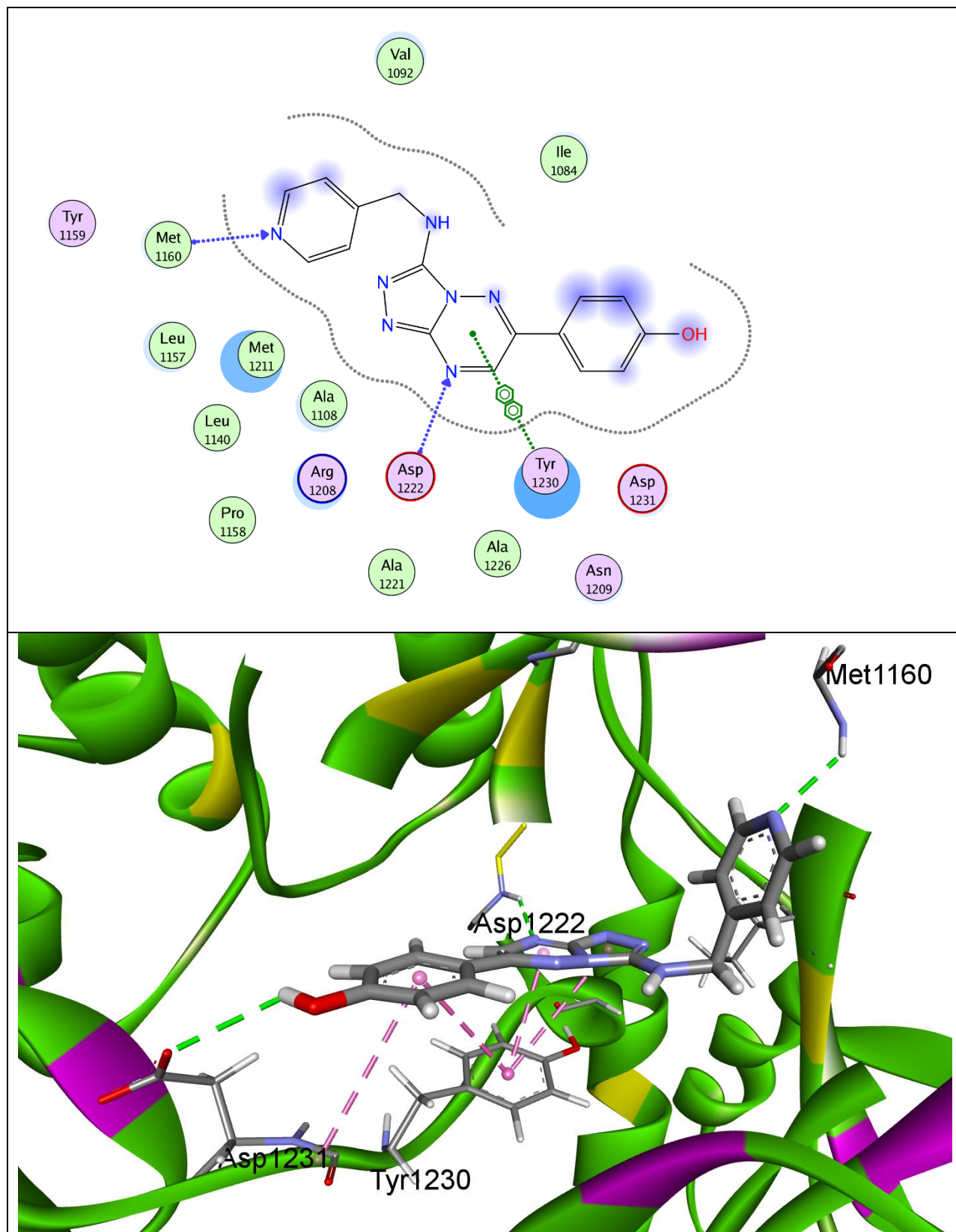


Figure 9. 2D (A) and 3D (B) presentations for the binding modes of **12g** in frame number 11 of the ATP binding

pocket of the c-Met receptor. Hydrogen bonds are shown as green dashes and π - π stacking interaction are shown as pink dashes.

3. Conclusions

In the present study, two series of NH-CH₂-linked triazolotriazine analogs were designed, synthesized, and tested for c-Met kinase and MDR reversal activity. The MTT assay indicated that most of the compounds have good-to-excellent activity. Interestingly, the inhibitory activity of **11f** and **12g** against the HepG2 cell line had IC₅₀ values of 5.736 and 3.059 μ M, respectively, which were comparable to that of the standard drug crizotinib (IC₅₀ =5.151 μ M). Compound **12g** emerged as the most potent c-Met kinase inhibitor with an IC₅₀ value of 0.052 μ M. It was found that all the synthesized compounds are non-toxic against the normal cell line, L929. Interestingly, **12g** can block both MDR1 and MRP1/2 pumps in the cancerous HepG2 and BxPC3 cells starting from the low concentrations of 3 and 0.3 μ M, respectively, and did not inhibit either pumps up to a concentration of 30 μ M in the noncancerous H69 cholangiocytes, suggesting **12g** as a potential selective anticancer agent. In addition, the resulting target compound **12g** benefits from improved water solubility due to the replacement of the sulfur atom by an NH group.

In summary, our study suggests that **12g** as a dual c-Met/MDR inhibitor may help us to develop novel leads for drug resistant cancer cells.

4. Experimental Section

4.1. General chemistry

The starting materials and all of the solvents and reagents utilized in this research were obtained from Merck or Sigma-Aldrich and used without any further purification. Crizotinib and HGF were obtained from Sigma-Aldrich (London, UK). Thin-layer chromatography (TLC) with Silica

gel 60 F254 (Merck, Darmstadt, Germany) was used to monitor reaction progress, and spots on plates were visualized with ultraviolet (UV) light (254 nm). Merck Kieselgel 60 (particle size 230-400 mesh) was used as a stationary phase in column chromatography. NMR spectra were recorded on either a Bruker 400 or 500 MHz instrument utilizing CDCl_3 or DMSO-d_6 solutions (reported in ppm). The Supplementary Material contains the synthesized compounds' instrumental data and NMR spectra. Analytical HPLC by a Knauer instrument was performed using a UV K-2600 detector and ODS-3 5 μm column for checking the purity of the compounds (>95%) for biological tests. Elemental analysis for C, H, and N was performed using a CHN analyzer (Heraeus, GmbH, Hanau, Germany). The results were found to be within $\pm 0.4\%$ of the theoretical values. The mass spectra of compounds were obtained using an G7081B instrument with Electro-ionization (20-70 eV) and Quadrupole Mass Selective Detector (Agilent Technologies, CA, USA).

4.2. General synthetic procedure

4.2.1 General procedure for the preparation of 3 - (Isothiocyanatomethyl) pyridine (3)

To a solution of the corresponding pyridine-3-ylmethanamine (49 mmol) in H_2O was added K_2CO_3 (98 mmol) and CS_2 (98 mmol), which were stirred overnight. Next, desulfurylation was carried out by using TCT (24.5 mmol) in CH_2Cl_2 in an ice bath. The ice bath was removed after 1 h, and the solution was stirred for 1 h at room temperature. Then, NaOH (6 N) solution was added dropwise to form a clear solution. Next, the extraction was carried out with dichloromethane (3 x 20 mL) and the solution concentrated under reduced pressure. In the final

step, purification was performed by column chromatography eluting with chloroform-ethyl acetate (90:10) [22].

Colorless oil, yield: 20%; ^1H NMR (400 MHz, CDCl_3) δ : 4.77 (s, 2H, CH_2), 7.37 (dd, $J = 8$ and 4.8 Hz, 1H, H-5), 7.72 (dt, $J = 8$ and 1.64 Hz, 1H, H-4), 8.59 (d, $J = 1.6$ Hz, 1H, H-6), 8.62 (dd, $J = 4.8$ Hz, $J = 1.2$ Hz, 1H, H-2), ^{13}C NMR (100 MHz, CDCl_3) δ : 46.42, 123.83, 130.18, 134.65, 137.08, 148.31, 149.88. Anal. Calcd for $\text{C}_7\text{H}_6\text{N}_2\text{S}$: C, 55.98; H, 4.03; N, 18.65%. Found: C, 56.02; H, 4.01; N, 18.71%.

4.2.2. Procedure for the preparation of Methyl (pyridin-4-ylmethyl) carbamodithioate (**4**)

Triethylamine (14.7 mmol) was added to the commercially available pyridine-4-ylmethanamine (9.8 mmol) in a mixture of diethyl ether and methanol (2:1). Afterwards, the reaction temperature was reduced to 0 °C and then a mixture of CS_2 (14.7 mmol) in ether was slowly added for 15 min. The resulting mixture was then stirred at room temperature for 24h. After this time, the solvent was evaporated to dryness and then replaced with methanol. The resulting mixture was kept at a temperature of -5 to -8 °C. Methyl iodide (14.7 mmol) in acetone was then added dropwise. After completely adding the methyl iodide, the reaction was kept at the same temperature for a further 10 min, and then the solution mixture was removed from the ice bath. The stirring was then continued for 1h at room temperature. Subsequently, the mixture was poured into an H_2O and ice bath to generate white solid particles. The resulting precipitate was filtered off and washed with H_2O . Finally, the title compound **4** was purified through column chromatography eluting with chloroform-methanol (99:1) [23].

White solid, yield: 75%, m.p.: 133-137°C; ^1H NMR (400 MHz, CDCl_3) δ : 2.68 (s, 3H, CH_3), 5.00 (d, $J = 5.6$ Hz, 2H, CH_2), 7.23 (d, $J = 5.6$ Hz, 2H, H-3 and H-5), 8.49 (d, $J = 4.8$ Hz, 2H, H-2 and H-6), 8.54 (brs, 1H, NH), ^{13}C NMR (100 MHz, CDCl_3) δ : 18.44, 49.21, 122.52, 146.11,

149.82, 200.84. Anal. Calcd for C₈H₁₀N₂S₂: C, 48.46; H, 5.08; N, 14.13%. Found: C, 48.51; H, 5.07; N, 14.15%.

4.2.4. General procedure for the synthesis of final derivatives (11a-f)

To a solution of 3-hydrazinyl-6-aryl-1,2,4-triazines (**10a-f**) (1eq) in absolute ethanol, 3-(isothiocyanatomethyl)pyridine **3** (1 eq) was added and then it was refluxed for 1 h. Dicyclohexylcarbodiimide (DCC) (1.5 eq) was then added, followed by reflux overnight. The solvent was evaporated and then purification by flash column chromatography, eluting with chloroform-methanol (95:5), yielded pure products **11a-f** [14].

4.2.5. General procedure for the synthesis of final derivatives (12a-f)

A mixture of 3-hydrazinyl-6-aryl-1, 2, 4-triazines (**10a-f**) (1eq) in absolute ethanol, was heated at reflux with methyl(pyridine-4-ylmethyl)carbamodithioate **4** (1 eq) overnight. Then, dicyclohexylcarbodiimide (DCC) (1.5 eq) was added, and the reaction mixture was heated at reflux for a further night. The resulting solution was concentrated, and then the crude products purified by column chromatography eluting (95:5) with chloroform-methanol to give desired products **12a-f** [14].

General procedure for the synthesis of final derivatives (11g, 12g)

A solution of **11f** (200 mg, 0.48 mmol) in HCl: CH₃COOH (1:1.5) was heated under reflux for 3 h. Then, the reaction was quenched with NaOH 50%. When the pH of the reaction reached 7, solid particles of **11g** appeared. The precipitated solid was filtered and then washed with plenty of water. Then, the final product of **11g** was purified by short column chromatography eluting with a chloroform-methanol (95:5) to give a pure compound of **11g**.

The final compound **12g** was synthesized using a method similar to that described above for the synthesis of **11g**, except that here the resulting precipitate was pure and did not require further purification [15].

4.2.4.1. *6-Phenyl-N-(pyridin-3-ylmethyl)-[1, 2, 4] triazolo [4, 3-b] [1, 2, 4] triazin-3-amine (11a)*. Orange solid, yield: 25%, m.p.: 184–186 °C; ¹H NMR (400 MHz, DMSO-d₆): δ: 4.66 (d, *J* = 6 Hz, 2H, CH₂), 7.36 (dd, *J* = 8 and 4.8 Hz, 1H, H-5 Py), 7.59-7.63 (m, 3H, H-3, H-4 and H-5 Ph), 7.80 (t, *J* = 6.4 Hz, 1H, NH), 7.86 (d, *J* = 7.6 Hz, 1H and H-4 Py), 8.19 (dd, *J* = 6.4 and 4.4 Hz, 2H, H-2 and H-6 Ph), 8.46 (d, *J* = 3.2 Hz, 1H, H-6 Py), 8.66 (s, 1H, H-2 Py), 9.07 (s, 1H, Triazine); ¹³C NMR (125 MHz, DMSO-d₆) δ: 43.89, 123.17, 126.66, 128.31, 129.01, 131.22, 133.46, 135.69, 143.83, 144.24, 146.39, 148.10, 148.52, 148.81; MS: (m/z, %): 303.1 (M⁺, 15), 199.1(7), 173.1 (100), 118.1 (26), Anal. Calcd for C₁₆H₁₃N₇: C, 63.36; H, 4.32; N, 32.32%. Found: C, 63.29; H, 4.33; N, 32.30%.

4.2.4.2. *N-(Pyridin-3-ylmethyl)-6-(p-tolyl)-[1,2,4]triazolo[4,3-b][1,2,4]triazin-3-amine (11b)*. Orange solid, yield: 30%, m.p.: 216 – 218 °C; ¹H NMR (400 MHz, CDCl₃) δ: 2.46 (s, 3H, CH₃), 4.96 (d, *J* = 6Hz, 2H, CH₂), 5.84 (t, 1H, *J*=6.4, NH), 7.35 (d, *J*= 8.4 Hz, 2H, H-3 and H-5 Ph), 7.49 (dd, *J*= 7.6 and *J*=5.2 Hz, 1H, H-5 Py), 7.87 (d, *J*= 8.4 Hz, 2H, H-2 and H-6 Ph), 8.19 (d, *J*= 8 Hz, 1H, H-4 Py), 8.58 (d, *J* = 4 Hz, 1H, H-6 Py), 8.78 (s, 1H, Triazine), 8.93 (s, 1H, H-2 Py); ¹³C NMR (125 MHz, CDCl₃) δ: 20.99, 43.98, 123.13, 126.53, 128.12, 129.76, 133.32, 135.54, 141.99, 143.85, 144.34, 146.35, 147.99, 148.77, 148.93; MS: (m/z, %): 317.2 (M⁺, 82),

199.1(9), 173.1 (100), 142.1(10), 118.1 (50). Anal. Calcd for C₁₇H₁₅N₇: C, 64.34; H, 4.76; N, 30.90%. Found: C, 64.48; H, 4.77; N, 30.87%.

4.2.4.3 6-(4-Methoxyphenyl)-N-(pyridin-3-ylmethyl)-[1, 2, 4] triazolo [4, 3-b] [1, 2, 4] triazin-3-amine (**11c**). Orange solid, yield: 30%, m.p.: 147–148°C; ¹H NMR (400 MHz, DMSO-d₆) δ: 3.85 (s, 3H, OCH₃), 4.65 (d, *J* = 6 Hz, 2H, CH₂), 7.14 (d, *J* = 8.8 Hz, 2H, H-3 and H-5 Ph), 7.35 (dd, *J* = 7.6 and 4.8 Hz, 1H, H-5 Py), 7.74 (t, *J* = 6 Hz, 1H, NH), 7.85(d, *J* = 7.6 Hz, 1H, H-4 Py), 8.15 (d, *J* = 9.2 Hz, 2H, H-2 and H-6 Ph), 8.46 (d, *J* = 3.6 Hz, 1H, H-6 Py), 8.66 (s, 1H, H-2 Py), 9.05 (s, 1H, Triazine); ¹³C NMR (125 MHz, DMSO-d₆) δ: 43.59, 55.96, 115.07, 123.84, 124.55, 129.41, 135.51, 135.90, 144.81, 145.64, 146.09, 148.65, 149.10, 149.60, 162.23; MS: (m/z, %): 333.3 (M⁺, 100), 191.2 (21), 173.2(5), 147.2 (35). Anal. Calcd for C₁₇H₁₅N₇O: C, 61.25; H, 4.54; N, 29.41%. Found: C, 61.19; H, 4.53; N, 29.47%.

4.2.4.4. 6-(4-Chlorophenyl)-N-(pyridin-3-ylmethyl)-[1,2,4]triazolo[4,3-b][1,2,4]triazin-3-amine (**11d**).

Orange solid, yield: 27%, m.p.: 188–189°C; ¹H NMR (400 MHz, DMSO-d₆) δ: 4.66 (d, *J* = 6.4 Hz, 2H, CH₂), 7.36 (dd, *J* = 7.2 and 4.8 Hz, 1H, H-5 Py), 7.70 (d, *J* = 8.4 Hz, 2H, H-3 and H-5 Ph), 7.81-7.86 (m, 2H, NH and H-4 Py), 8.21 (d, *J* = 8.8 Hz, 2H, H-2 and H-6 Ph), 8.46 (d, *J* = 4.8 Hz, 1H, H-6 Py), 8.66 (s, 1H, H-2 Py), 9.07(s, 1H, Triazine); ¹³C NMR (125 MHz, DMSO-d₆) δ: 43.98, 123.15, 127.89, 129.37, 132.58, 133.23, 135.56, 137.87, 143.15, 144.13, 145.40, 148.01, 148.77, 148.90; MS: (m/z, %): 337.2 (M⁺, 68), 339 (M⁺², 21), 284.3(8), 256.3(10),

173.2(4), 149.1 (16), 111.2 (21) , 57.2 (100). Anal. Calcd for C₁₆H₁₂ClN₇: C, 56.90; H, 3.58; N, 29.03%. Found: C, 56.81; H, 3.59; N, 29.11%.

4.2.4.5. *6-(4-Bromophenyl)-N-(pyridin-3-ylmethyl)-[1,2,4]triazolo[4,3-b][1,2,4]triazin-3-amine (11e)*.

Orange solid, yield: 28 %, m.p.: 219–221°C; ¹H NMR (400 MHz, DMSO-d₆) δ: 4.66 (d, *J* = 6 Hz, 2H, CH₂), 7.36 (dd, *J* = 8 and 4.8 Hz, 1H, H-5 Py), 7.83(d, *J*= 8.8 Hz, 2H, H-3 and H-5 Ph), 7.81-7.86 (m, 2H, NH, H-4 Py), 8.13 (d, *J*= 8.8 Hz, 2H, H-2 and H-6 Ph), 8.46 (d, *J* = 6 Hz, 1H, H-6 Py), 8.66 (s, 1H, H-2 Py), 9.06 (s, 1H, Triazine); ¹³C NMR (125 MHz, DMSO-d₆) δ: 43.95, 123.18, 126.27, 128.05, 129.51, 132.35, 133.27, 135.63, 143.12, 144.12, 145.50, 148.03, 148.71, 148.86; MS: (m/z, %): 381.1 (M⁺, 9), 383.1 (M⁺², 8), 173.2 (100), 157(10), 140.2(12), , 118.1 (20). Anal. Calcd for C₁₆H₁₂ BrN₇: C, 50.28; H, 3.16; N, 25.65%. Found: C, 50.37; H, 3.17; N, 25.60%.

4.2.4.6 *6-(4-(Benzyloxy)phenyl)-N-(pyridin-3-ylmethyl)-[1,2,4]triazolo[4,3-b][1,2,4]triazin-3-amine (11f)*. Orange solid, yield: 35 %, m.p.: 203- 205°C; ¹H NMR (400 MHz, DMSO-d₆) δ: 4.68 (d, *J* = 6 Hz, 2H, CH₂), 5.23 (s, 2H, CH₂ Benzyl), 7.23 (d, *J*= 8.8Hz, 2H, H-3 and H-5 Ph), 7.36 (d, *J*= 7.2 Hz, 1H, H-5 Py) 7.39- 7.50 (m, 5H, H-2, H-3, H-4 , H-5 and H-6 Benzyl), 7.80 (t, *J*= 6.8Hz, 1H, NH), 7.99 (d, *J* = 7.6 Hz, 1H, H-4 Py), 8.16 (d, *J* = 8.8 Hz, 2H, H-2 and H-6 Ph), 8.53 (d, *J* = 4 Hz, 1H, H-6 Py), 8.72 (s, 1H, H-2 Py), 9.06 (s, 1H, Triazine); ¹³C NMR (125 MHz, DMSO-d₆) δ: 43.99, 69.80, 115.40, 123.18, 123.46, 126.96, 127.83, 128.24, 128.27, 133.43, 135.54, 135.70, 143.73, 144.34, 145.92, 147.95, 148.63, 148.82, 161.21; MS: (M/z, %):

409.3 (M^+ , 22), 290.1(6), 173.1 (49), 91.2 (100). Anal. Calcd for $C_{23}H_{19}N_7O$: C, 67.47; H, 4.68; N, 23.95%. Found: C, 67.59; H, 4.69; N, 23.88%.

4.2.4.7. 4-(3-((Pyridin-3-ylmethyl)amino)-[1,2,4]triazolo[4,3-b][1,2,4]triazin-6-yl)phenol (**11g**).

Yellow solid, yield: 50 %, m.p.: 118-120°C; 1H NMR (400 MHz, DMSO- d_6) δ : 4.64 (d, J = 5.6 Hz, 2H, CH_2), 6.95 (d, J = 8 Hz, 2H, H-3 and H-5 Ph), 7.35 (t, J = 5.2 Hz, 1H, H-5 Py), 7.70 (t, J = 6.4 Hz, 1H, NH), 7.85 (d, J = 7.2 Hz, 1H, H-4 Py), 8.05 (d, J = 8 Hz, 2H, H-2 and H-6 Ph), 8.46 (d, J = 4 Hz, 1H, H-6 Py), 8.66 (s, 1H, H-2 Py), 9.00 (s, 1H, Triazine), 10.27 (s, 1H, OH); ^{13}C NMR (100 MHz, DMSO- d_6) δ : 43.59, 116.44, 122.93, 123.84, 129.53, 135.52, 135.90, 144.83, 145.64, 146.28, 148.64, 149.07, 149.61, 160.96; MS: (m/z, %): 319.2 (M^+ , 20), 209.2 (19), 192.2(18), 173.2 (4), 91.2 (100). Anal. Calcd for $C_{16}H_{13}N_7O$: C, 60.18; H, 4.10; N, 30.70%. Found C, 60.29; H, 4.11; N, 30.65%.

4.2.5.1. 6-Phenyl-N-(pyridin-4-ylmethyl)-[1,2,4]triazolo[4,3-b][1,2,4]triazin-3-amine (**12a**).

Orange solid, yield: 20 %, m.p.: 209-211°C; 1H NMR (400 MHz, DMSO- d_6) δ : 4.67 (d, J = 6 Hz, 2H, CH_2), 7.41 (d, J = 6 Hz, 2H, H-3 and H-5 Py), 7.60-7.63 (m, 3H, H-3, H-4 and H-5 Ph), 7.88 (t, J = 6 Hz, 1H, NH), 8.19 (dd, J = 7.2 and 3.6 Hz, 2H, H-2 and H-6 Ph), 8.50 (d, J = 6 Hz, 2H, H-2 and H-6 Py), 9.09 (s, 1H, Triazine); ^{13}C NMR (100 MHz, DMSO- d_6) δ : 44.88, 122.80, 127.77, 129.61, 131.74, 132.34, 142.05, 144.85, 145.78, 146.50, 149.16, 149.93; MS: (m/z, %): 303.1 (M^+ , 91), 199.1 (18), 173.1 (100), 128.1 (27), 104.1(48). Anal. Calcd for $C_{16}H_{13}N_7$: C, 63.36; H, 4.32; N, 32.32%. Found: C, 63.39; H, 4.33; N, 32.38%.

4.2.5.2. *N*-(Pyridin-4-ylmethyl)-6-(*p*-tolyl)-[1,2,4]triazolo[4,3-*b*][1,2,4]triazin-3-amine (**12b**).

Orange solid, yield: 25 %, m.p.: 198-200 °C; ¹H NMR (400 MHz, CDCl₃) δ: 2.47 (s, 3H, CH₃), 4.89 (d, *J* = 6.4 Hz, 2H, CH₂), 5.47 (t, *J* = 6.4 Hz, 1H, NH), 7.37 (d, *J* = 8 Hz, 2H, H-3 and H-5 Ph) 7.40 (d, *J* = 6 Hz, 2H, H-3 and H-5 Py), 7.86 (d, *J* = 8.4 Hz, 2H, H-2 and H-6 Ph), 8.59 (d, *J* = 5.6 Hz, 2H, H-2 and H-6 Py), 8.79 (s, 1H, Triazine); ¹³C NMR (100 MHz, CDCl₃) δ: 29.70, 45.69, 122.52, 127.05, 128.53, 130.30, 142.58, 144.53, 144.87, 146.94, 147.32, 148.45, 150.03; MS: (m/z, %): 317.2 (M⁺, 40), 279.1 (12), 173.1(25), 149.1 (67), 43.2 (100). Anal. Calcd for C₁₇H₁₅N₇: C, 64.34; H, 4.76; N, 30.90%. Found: C, 64.22; H, 4.75; N, 30.84%.

4.2.5.3. 6-(4-Methoxyphenyl)-*N*-(pyridin-4-ylmethyl)-[1, 2, 4]triazolo[4,3-*b*][1,2,4]triazin-3-amine (**12c**). Orange solid, yield: 25 %, m.p.: 165-167 °C; ¹H NMR (400 MHz, DMSO-*d*₆) δ:

3.86 (s, 3H, OCH₃), 4.66 (d, *J* = 6 Hz, 2H, CH₂), 7.15 (d, *J* = 8.8 Hz, 2H, H-3 and H-5 Ph), 7.41 (d, *J* = 6 Hz, 2H, H-3 and H-5 Py), 7.81 (t, *J* = 6 Hz, 1H, NH), 8.17 (d, *J* = 8.8 Hz, 2H, H-2 and H-6 Ph), 8.50 (d, *J* = 6 Hz, 2H, H-2 and H-6 Py), 9.06(s, 1H, Triazine); ¹³C NMR (100 MHz, DMSO-*d*₆) δ: 44.89, 55.99, 115.08, 122.79, 124.54, 129.42, 144.82, 145.67, 146.11, 149.11, 149.20, 149.91, 162.24; MS: (m/z, %): 333.2 (M⁺, 100), 242.2 (17), 199.1 (22), 173.1 (86), 158.1 (18), 146.1 (25) , 134.1 (58). Anal. Calcd for C₁₇H₁₅N₇O: C, 61.25; H, 4.54; N, 29.41%. Found: C, 61.14; H, 4.55; N, 29.37%.

4.2.5.4. 6-(4-Chlorophenyl)-*N*-(pyridin-4-ylmethyl)-[1,2,4]triazolo[4,3-*b*][1,2,4]triazin-3-amine (**12d**).

Orange solid, yield: 22 %, m.p.: 215-217 °C; ¹H NMR (400 MHz, DMSO-*d*₆) δ: 4.67 (d, *J* = 6.4 Hz, 2H, CH₂), 7.41 (d, *J* = 6 Hz, 2H, H-3 and H-5 Py), 7.70 (d, *J* = 8.8 Hz, 2H, H-3 and H-5 Ph), 7.91 (t, *J* = 6 Hz, 1H, NH), 8.22 (d, *J* = 8.8 Hz, 2H, H-2 and H-6 Ph), 8.50 (d, *J* = 6 Hz, 2H, H-2 and H-6 Py), 9.08(s, 1H, Triazine); ¹³C NMR (100 MHz, DMSO-*d*₆) δ: 44.85, 122.79,

129.52, 129.69, 131.25, 136.68, 144.74, 145.54, 145.57, 149.10, 149.16, 149.93; MS: (m/z, %): 337.2 (M⁺, 68), 339.2 (M⁺², 22), 246.1(20), 199.1 (16), 173.1 (100), 163.2 (13), 152.1(20), 138.1(46), 111.1 (29). Anal. Calcd for C₁₆H₁₂ ClN₇: C, 56.90; H, 3.58; N, 29.03%. Found: C, 56.79; H, 3.57; N, 29.09%.

4.2.5.5. *6-(4-Bromophenyl)-N-(pyridin-4-ylmethyl)-[1,2,4]triazolo[4,3-b][1,2,4]triazin-3-amine (12e)*. Orange solid, yield: 27 %, m.p.: 210-212 °C; ¹H NMR (400 MHz, DMSO-d₆) δ: 4.66 (d, *J* = 6 Hz, 2H, CH₂), 7.41 (d, *J* = 6 Hz, 2H, H-3 and H-5 Py), 7.84 (d, *J* = 8.8 Hz, 2H, H-3 and H-5 Ph), 7.91 (t, *J* = 6 Hz, 1H, NH), 8.14 (d, *J* = 8.8 Hz, 2H, H-2 and H-6 Ph), 8.50 (d, *J* = 6 Hz, 2H, H-2 and H-6 Py), 9.07(s, 1H, Triazine); ¹³C NMR (100 MHz, DMSO-d₆) δ: 44.85, 122.79, 125.61, 129.69, 131.60, 132.61, 144.75, 145.49, 145.69, 149.11, 149.16, 149.91; MS: (m/z, %): 381.1 (M⁺, 39), 383.1 (M⁺², 7), 199.1(19), 184 (30), 173.1 (100), 158 (17), 127.1 (30). Calcd for C₁₆H₁₂ BrN₇: C, 50.28; H, 3.16; N, 25.65%. Found: C, 50.13; H, 3.17; N, 25.60%.

4.2.5.6. *6-(4-(Benzyloxy)phenyl)-N-(pyridin-4-ylmethyl)-[1,2,4]triazolo[4,3-b][1,2,4]triazin-3-amine (12f)*. Orange solid, yield: 30 %, m.p.: 183-185 °C; ¹H NMR (400 MHz, DMSO-d₆) δ: 4.66 (d, *J* = 6.4 Hz, 2H, CH₂), 5.23 (s, 2H, CH₂ Benzyl), 7.23(d, *J* = 8.8 Hz, 2H, H-3 and H-5 Ph), 7.34 (d, *J* = 7.2 Hz, 1H, H-4 Benzyl), 7.37-7.43 (m, 4H, H-3 and H-5 Py, H-3, and H-5 Benzyl), 7.49 (d, *J* = 7.2 Hz, 2H, H-2 and H-6, Benzyl), 7.82 (t, *J* = 6.4 Hz, 1H, NH), 8.16 (d, *J* = 8.8Hz, 2H, H-2 and H-6 Ph), 8.50 (d, *J* = 4.8Hz, 2H, H-2 and H-6 Py), 9.06(s, 1H, Triazine); ¹³C NMR (100 MHz, DMSO-d₆) δ: 44.89, 69.95, 115.93, 122.80, 124.75, 128.28, 128.47, 128.96, 129.44, 137.04, 144.82, 145.67, 146.09, 149.11, 149.21, 149.90, 161.30; MS: (m/z, %): 409.3 (M⁺, 34), 318.2 (31), 173.1 (9), 91.2 (100). Anal. Calcd for C₂₃H₁₉ N₇O: C, 67.47; H, 4.68; N, 23.95%. Found: C, 67.59; H, 4.67; N, 24.01%.

4.2.5.7. 4-(3-((Pyridin-4-ylmethyl)amino)-[1,2,4]triazolo[4,3-b][1,2,4]triazin-6-yl)phenol (**12g**).

Yellow solid, yield: 55 %, m.p.: 108-110 °C; ¹H NMR (400 MHz, DMSO-d₆) δ: 4.65 (d, J = 6 Hz, 2H, CH₂), 6.97 (d, J = 8.4 Hz, 2H, H-3 and H-5 Ph), 7.42 (d, J = 2.4, 2H, H-3 and H-5Py), 7.77(t, J = 6 Hz, 1H, NH), 8.06 (d, J = 8.8Hz, 2H, H-2 and H-6 Ph), 8.53(d, J = 3.2 Hz, 2H, H-2 and H-6 Py), 9.02 (s, 1H, Triazine), 10.30 (s, 1H, OH); ¹³C NMR (100 MHz, DMSO-d₆) δ: 44.90, 116.47, 122.93, 129.19, 129.54, 144.85, 145.69, 146.32, 149.08, 149.26, 149.86, 160.99; MS: (m/z, %): 319.2 (M⁺, 25), 190.2(9), 173.1(5), 91.2 (100). Anal. Calcd for C₁₆H₁₃N₇O: C, 60.18; H, 4.10; N, 30.70%. Found: C, 60.30; H, 4.11; N, 30.64%.

4.3. Calculation of water solubility

Standard sample solutions of **2**, **11b** and **12g** with a concentration of 0.1 mg/mL were prepared by dissolving each compound **2**, **11b** and **12g** (1mg) in HPLC grade methanol (10 mL). The maximum absorbance of compounds **2**, **11b** and **12g** were measured by UV–Visible spectroscopy (Series UV/Vis spectrophotometer PG Instrument Ltd., T80+, China) at wavelengths of 236, 242 and 248 nm, respectively. Saturated solutions were prepared by adding excess compounds **2**, **11b** and **12g** to 2 mL of deionized water. The solutions containing solid excess of the samples were then capped, sonicated for 20 min and centrifuged at 1600 rpm for 30 min. The supernatants were filtered using a 0.45 μm syringe filter. The absorbance of the saturated water solutions of **2**, **11b** and **12g** was measured. The concentrations of compounds **2**, **11b** and **12g** in aqueous solution were calculated using the following equation:

$$C' = A' \times C/A$$

C = concentration of standard sample solution (mg/L), A = absorbance of standard sample solution, A' = absorbance of saturated sample solution, C' = concentration of water solution of each compound **2**, **11b** and **12g** (mg/L) [24].

4.4. Single-crystal X-ray crystallography

A crystal of compound **11c** was placed in Paratone-N oil and flash cooled to 100 K in a nitrogen stream in an Oxford Cryostream cooler. A Rigaku XtaLAB Synergy diffractometer (Cu K α radiation (λ = 1.54184 Å) was used to collect single-crystal X-ray intensity data (Table S1). The data were reduced using *CrysAlisPro* software [25]. The structure was solved by applying the program *Superflip* [26], and all non-hydrogen atoms located. Subsequently, the *CRYSTALS* suite of programs was utilized to perform least-squares refinements against *F* [27]. The non-hydrogen atoms were refined anisotropically. All the hydrogen atoms were located in difference Fourier maps. The hydrogen atom (H151) attached to nitrogen (N15) was refined isotropically. The hydrogen atoms attached to carbon were geometrically placed with a C-H distance of 0.95 Å and a Uiso value ~1.2 times that of the Uequiv value of the parent C atom. These hydrogen atom positions were then refined using riding constraints.

4.5. HGF-induced proliferation assay

MCF-7, MDA-MB-231, HepG2, HT29 and L929 cell lines were purchased from ATCC. The MTT assay was used to evaluate the anti-proliferative activities of the compounds as well as the positive control crizotinib (Sigma, PZ0191) against MCF-7, MDA-MB-231, HepG2, and HT29 cell lines. The cancer cell lines were grown in Dulbecco's modified Eagle's medium (DMEM) supplemented with 10% FBS, 1% L-glutamine, and 1% antibiotics and retained at 37 °C in a

humid environment with 5% CO₂. Cancer cells were seeded in 96-well plates at 4000 cells per well. Cells were starved for 24 hours in an FBS-free medium and recombinant human HGF (40 ng/ml) (Sigma, H5791), then treated with test compounds at various concentrations for 72 hours at 37 °C. Following the incubation period, each well received 10 µL of MTT reagent (5 mg/ml). 100µ L DMSO was used to dissolve MTT formazan crystals. Using a Biotek Power Wave XS microplate reader, the relative cell viability was calculated by comparing the absorbance values at 690 nm (for MTT formazan absorbance) and 570 nm (for reference wavelength) of the treated and untreated control groups. GraphPad Prism was also utilized to estimate the IC₅₀ values.

4.6. c-Met inhibition assay

The c-Met kinase inhibitory activity was measured using the Met Kinase Enzyme System (V3361, Promega, USA) with an ADP-Glo assay. Screening for kinase inhibitory activity of molecules at doses ranging from 0.1 to 50 µM was done in duplicate, as recommended by the manufacturer. Reactions containing kinase buffer, 10 µM ATP, 0.2 µg/µl poly (Glu, Tyr) 4:1 peptide substrate, and 4 ng c-Met kinase enzyme were set up on 384-well Lumox (Sarstedt) plates for 1 h at room temperature. In order to quantify the amount of ADP produced during kinase activities, an ADP-Glo kinase assay was employed. After adding 5 µl of ADP- GloTM reagent to each well and leaving the plate at room temperature for 40 minutes, the kinase reaction was stopped. The luminescence was measured using a multimode plate reader after adding 10 µL of kinase detection reagent and 30 minutes of additional incubation (BMG Labtech Omega FLUOstar). The IC₅₀ values were computed using the GraphPad Prism software.

4.7. Multidrug resistance assay

4.7.1. Chemicals

Verapamil hydrochloride ($\geq 98.0\%$ purity) was purchased from Merck Life Science S.r.l. (Milan, Italy), while MK571 ($\geq 96.0\%$ purity) from Santa Cruz Biotechnology, Inc. (California, USA). Dulbecco's Modified Eagle's medium (DMEM), Roswell Park Memorial Institute (RPMI) 1640 culture medium, fetal bovine serum, buffer and cofactors were from Aurogene S.r.l. (Rome, Italy). **12g**, verapamil hydrochloride and MK571 were dissolved in DMSO (100% v/v) and administered up to a maximum 1% v/v concentration of the solvent, which was nontoxic to cells.

4.7.2. Cell lines

Human hepatoma HepG2 cells were purchased from American Type Culture Collection (ATCC), pancreatic adenocarcinoma (Bx-PC3) cells from Interlab Cell Line Collection (IRCCS San Martino Policlinico Hospital, Genoa, Italy), while noncancerous H69 intrahepatic cholangiocytes were a kind gift from Prof. Mancinelli R. (Department of Anatomical, Histological, Forensic and Orthopedic Sciences, Sapienza University of Rome) and Prof. G. Alpini (Indiana University School of Medicine, Indianapolis, IN). The cell lines were grown using appropriate media and co-factors under standard conditions (37 °C and 5% CO₂), according to previous studies [16]. The growth media were changed twice per week, as recommended by the suppliers; when the cells were around 80% confluent, subcultures were prepared.

4.7.3. ABC-mediated drug efflux assay

In order to select the highest nontoxic concentrations to be tested in the efflux assay, a preliminary cytotoxicity assay, wherein confluent cells (2×10^4 cells/well) were treated with progressive dilutions of the substance **12g** for 30 minutes, was performed. The effect of the

treatment on the cell viability was measured by the MTT assay and a higher than 30% reduction of cell viability was considered as a significant cytotoxic effect [16].

The ability of the test compound **12g** to affect the efflux mediated by MDR1 and MRP transporters was evaluated at nontoxic concentrations, according to previously published methods [18] with minor changes. Briefly, confluent cells (2×10^4 cells/well) were treated with progressive concentrations of **12g**, or the positive controls verapamil and MK571 (2 μ M), both in the absence and presence of suitable fluorescent probes (i.e., 1 μ M rhodamine 123 for MDR1 and 0.05 μ M calcein acetoxymethyl ester for MRP1 and MRP2) for 30 minutes; then, the fluorescence was measured at excitation and emission wavelengths of 485 nm and 535 nm for both probes, using a Cytation 1 Cell Imaging Multimode Reader (Biotech, USA). Results were normalized to viable cells and expressed as a percentage of the negative control.

4.7.4. Immunofluorescence analysis of Pgp, MRP1 and MRP2 transporter expression

To perform the analysis, confluent cells were grown in 24-well plates (4×10^4 cells/well), then treated with **12g** (3 μ M), the standard inhibitors verapamil (2 μ M) and MK571 (2 μ M) and their vehicles for 24 h. After treatment, the cells were fixed in pure methanol, washed and then, stained with suitable primary anti-MDR1/ABCB1 (mAB #13342, Cell Signaling Technology; dilution factor 1:400), anti-MRP1 (sc-18835, Santa Cruz Biotechnology Inc.; dilution factor 1:500) and anti-MRP2 (bs-1092R, Bioss Inc.; dilution factor 1:200) antibodies, followed by specific secondary antibodies (dilution factor 1:800) and Hoechst 33258 nucleic acid dye (1 μ g/mL). A Cytation 1 Cell Imaging Multimode Reader (Biotech, USA) was used to evaluate the expression and localization of Pgp, MRP1, and MRP2 pumps into cells, while the fluorescence

intensity was determined by Gen5™ Microplate Reader and Imager Software 3.11, according to previous studies [16].

4.7.5. Statistical analysis

Data from at least three independent experiments, each one including at least three technical replicates per treatment, were pooled, analyzed by GraphPad Prism™ (Version 6.00) software (GraphPad Software, Inc., San Diego, California, USA) and expressed as mean \pm standard error (SE). The significance of the response (p value < 0.05) with respect to control was evaluated by the one-way analysis of variance (one-way ANOVA), followed by Dunnett's Multiple Comparison Post Test or by Student t -test.

4.8. In silico study

Docking study was performed by AutoDock Vina v1.2.3 and the PDB code of 5EOB was used as the c-Met tyrosine kinase receptor. The validation of the docking method was accomplished by redocking of the cognate ligand of the PDB file (Figure S4). The RMSD of the docked conformer and its binding conformation is in Figure S5 of Supplementary Material. Correspondingly, compound **12g** was docked into the ATP binding site of the receptor and the following parameters were used as configuration of the docking method. Center of the grid was set to: $x = 1.719$, $y = 10.198$, $z = 28.542$, the grid dimensions were set to: $x = 20.0$, $y = 20.0$, $z = 20.0$ and the exhaustiveness was set to 32.

GROMACS version 2020 installed on a Linux workstation was used for dynamics simulation of compounds in the binding site in explicit water model TIP3P and Amber99SB-ILDN force field was used for topology generation. Topology of ligands were generated by ACPYPE and GAFF was used for ligand topology generation. Ligand atomic charges were calculated using PM3 in

Gaussian 09. The topology and coordinate files for the protein were generated using pdb2gmx program of GROMACS package taking parameters from the Amber99SB-ILDN force field. The coordinate and topology files of the protein and the ligands were then merged to obtain the final starting structure and topology file for each complex.

The complex was centered in a dodecahedron periodic box and solvated by the addition of water molecules (Simple point charge model). The total charge of the system was then neutralized by addition of sodium and chloride ions as required. Sequentially, energy minimization was performed by steepest descent algorithm. The system was then gradually heated to 300 K and was equilibrated 100 ps using the NVT (constant volume and temperature) ensemble with position restraint for the heavy atoms followed by 100 ps equilibration in the NPT (constant pressure and temperature) ensemble at 1 atm. Both temperature and pressure were regulated using the Berendsen algorithm. Finally, the full system was subjected to 20 ns MD simulation with a 2 fs time step interval. The temperature and pressure were maintained at 300 K and 1 atm using the v-rescale temperature and Parrinello-Rahman pressure coupling method. The short-range non-bonded interactions were computed for the atom pairs within the cut-off of 1.2 nm, while the long-range electrostatic interactions were calculated using Particle-Mesh-Ewald summation method with fourth-order cubic interpolation and 1.2 Å grid spacing. All h-bonds were constrained using the parallel LINCS method. The last 10 frames of the equilibrated and stable ligand-protein complex were extracted and analyzed for the necessary interactions [28]. Visualization of the interactions was performed by Discovery Studio Visualizer v17.2.0 (2016, Dassault Systems Biovia Corp).

Supplementary material

The mass, ^1H and ^{13}C NMR spectra of the target compounds **11a-g** and **12a-g** are provided in the Supplementary material.

Acknowledgment

This study is related to the PhD thesis of Zahra Zakeri Khatir and was supported by grant no. 4940 from the research council of Mazandaran University of Medical Sciences, Sari, Iran. The University of Reading is thanked for use of the X-ray diffraction instrument in the Chemical Analysis Facility (CAF) and the help of Mr Nicholas Spencer.

Author Contributions

Synthesis, characterization of the compounds and chemistry part was performed by ZZK. Multidrug resistance efflux assay was done by ADS and EP. HGF-induced proliferation and c-Met kinase assays were performed by TTK and AE. X-ray analysis was done by AMC. HI designed, conceptualized and supervised the study. MV contributed in the editing of the manuscript.

Conflict of interest

The authors declare no conflict of interest.

References:

- [1] C. Chu, Z. Rao, Q. Pan, and W. Zhu, "An updated patent review of small-molecule c-Met kinase inhibitors (2018-present)," *Expert Opin. Ther. Pat.*, vol. 32, no. 3, pp. 279–298, 2022.
- [2] K. Engle and G. Kumar, "Cancer multidrug-resistance reversal by ABCB1 inhibition: A recent update," *Eur. J. Med. Chem.*, p. 114542, 2022.
- [3] T. Bin Emran *et al.*, "Multidrug resistance in cancer: understanding molecular mechanisms, immunoprevention and therapeutic approaches," *Front. Oncol.*, vol. 12, p.

891652, 2022.

- [4] L. Zinzi, E. Capparelli, M. Cantore, M. Contino, M. Leopoldo, and N. A. Colabufo, “Small and innovative molecules as new strategy to revert MDR,” *Front. Oncol.*, vol. 4, p. 2, 2014.
- [5] S. S. Hosseini Balef, M. Piramoon, S. J. Hosseinimehr, and H. Irannejad, “In vitro and in silico evaluation of P-glycoprotein inhibition through ^{99m}Tc-methoxyisobutylisonitrile uptake,” *Chem. Biol. & drug Des.*, vol. 93, no. 3, pp. 283–289, 2019.
- [6] A. Di Sotto *et al.*, “Potentiation of low-dose doxorubicin cytotoxicity by affecting p-glycoprotein through caryophyllane sesquiterpenes in hepg2 cells: An in vitro and in silico study,” *Int. J. Mol. Sci.*, vol. 21, no. 2, p. 633, 2020.
- [7] Q. Cui *et al.*, “Glesatinib, a c-MET/SMO dual inhibitor, antagonizes P-glycoprotein mediated multidrug resistance in cancer cells,” *Front. Oncol.*, vol. 9, p. 313, 2019.
- [8] Z.-X. Wu *et al.*, “Tivantinib, A c-met inhibitor in clinical trials, is susceptible to ABCG2-mediated drug resistance,” *Cancers (Basel)*, vol. 12, no. 1, p. 186, 2020.
- [9] W. Zhou *et al.*, “Crizotinib (PF-02341066) reverses multidrug resistance in cancer cells by inhibiting the function of P-glycoprotein,” *Br. J. Pharmacol.*, vol. 166, no. 5, pp. 1669–1683, 2012.
- [10] Z.-X. Wu *et al.*, “Tepotinib reverses ABCB1-mediated multidrug resistance in cancer cells,” *Biochem. Pharmacol.*, vol. 166, pp. 120–127, 2019.
- [11] S. Dadashpour, T. T. Küçük\il\inç, A. Ercan, S. J. Hosseinimehr, N. Naderi, and H. Irannejad, “Synthesis and anticancer activity of benzimidazole/benzoxazole substituted triazolotriazines in hepatocellular carcinoma,” *Anti-Cancer Agents Med. Chem. (Formerly Curr. Med. Chem. Agents)*, vol. 19, no. 17, pp. 2120–2129, 2019.

- [12] S. Dadashpour *et al.*, “Discovery of novel 1, 2, 4-triazolo-1, 2, 4-triazines with thiomethylpyridine hinge binders as potent c-Met kinase inhibitors,” *Future Med. Chem.*, vol. 11, no. 10, pp. 1119–1136, 2019.
- [13] Z. Song *et al.*, “Highly chemoselective trichloroacetimidate-mediated alkylation of ascomycin: A convergent, practical synthesis of the immunosuppressant L-733,725,” *J. Org. Chem.*, vol. 64, no. 6, pp. 1859–1867, 1999.
- [14] I. M. Labouta, N. H. Eshba, and H. M. Salama, “Synthesis of some substituted triazolo [4, 3-b][1, 2, 4] triazines as potential anticancer agents,” *Monatshefte für Chemie/Chemical Mon.*, vol. 119, no. 5, pp. 591–596, 1988.
- [15] T. Storr *et al.*, “Vanadyl- Thiazolidinedione combination agents for diabetes therapy,” *Bioconjug. Chem.*, vol. 14, no. 1, pp. 212–221, 2003.
- [16] S. Di Giacomo *et al.*, “Sorafenib chemosensitization by caryophyllane sesquiterpenes in liver, biliary, and pancreatic cancer cells: The role of STAT3/ABC transporter axis,” *Pharmaceutics*, vol. 14, no. 6, p. 1264, 2022.
- [17] U. Hoffmann and H. K. Kroemer, “The ABC transporters MDR1 and MRP2: multiple functions in disposition of xenobiotics and drug resistance,” *Drug Metab. Rev.*, vol. 36, no. 3–4, pp. 669–701, 2004.
- [18] B. Noma *et al.*, “Expression of multidrug resistance-associated protein 2 is involved in chemotherapy resistance in human pancreatic cancer,” *Int. J. Oncol.*, vol. 33, no. 6, pp. 1187–1194, 2008.
- [19] P. Sharma, N. Singh, and S. Sharma, “ATP binding cassette transporters and cancer: Revisiting their controversial role,” *Pharmacogenomics*, vol. 22, no. 18, pp. 1211–1235, 2021.

- [20] J.-Q. Wang *et al.*, “Multidrug resistance proteins (MRPs): Structure, function and the overcoming of cancer multidrug resistance,” *Drug Resist. Updat.*, vol. 54, p. 100743, 2021.
- [21] M. Drozdziak *et al.*, “Protein abundance of hepatic drug transporters in patients with different forms of liver damage,” *Clin. Pharmacol. & Ther.*, vol. 107, no. 5, pp. 1138–1148, 2020.
- [22] N. Sun *et al.*, “A general and facile one-pot process of isothiocyanates from amines under aqueous conditions,” *Beilstein J. Org. Chem.*, vol. 8, no. 1, pp. 61–70, 2012.
- [23] W. T. Ashton *et al.*, “Nonpeptide angiotensin II antagonists derived from 4H-1, 2, 4-triazoles and 3H-imidazo [1, 2-b][1, 2, 4] triazoles,” *J. Med. Chem.*, vol. 36, no. 5, pp. 591–609, 1993.
- [24] K.-C. Lee, E. Venkateswararao, V. K. Sharma, and S.-H. Jung, “Investigation of amino acid conjugates of (S)-1-[1-(4-aminobenzoyl)-2, 3-dihydro-1H-indol-6-sulfonyl]-4-phenyl-imidazolidin-2-one (DW2282) as water soluble anticancer prodrugs,” *Eur. J. Med. Chem.*, vol. 80, pp. 439–446, 2014.
- [25] “CrysAlisPro.” Rigaku Oxford Diffraction Ltd., Oxfordshire, England, 2019.
- [26] L. Palatinus and G. Chapuis, “SUPERFLIP a computer program for the solution of crystal structures by charge flipping in arbitrary dimensions,” *J. Appl. Crystallogr.*, vol. 40, no. 4, pp. 786–790, Aug. 2007, doi: 10.1107/S0021889807029238.
- [27] P. W. Betteridge, J. R. Carruthers, R. I. Cooper, K. Prout, and D. J. Watkin, “CRYSTALS version 12: software for guided crystal structure analysis,” *J. Appl. Crystallogr.*, vol. 36, no. 6, 2003.
- [28] M. Valipour, S. Di Giacomo, A. Di Sotto, and H. Irannejad, “Discovery of Chalcone-

Based Hybrid Structures as High Affinity and Site-Specific Inhibitors against SARS-CoV-2: A Comprehensive Structural Analysis Based on Various Host-Based and Viral Targets,” *Int. J. Mol. Sci.*, vol. 24, no. 10, May 2023, doi: 10.3390/ijms24108789.